Interactions of dispersive shock waves

M.A. Hoefer[a,*], M.J. Ablowitz[b]

[a] *National Institute of Standards and Technology, Electromagnetics Division, Boulder, CO 80305, USA*
[b] *Department of Applied Mathematics, University of Colorado, Boulder, CO 80309-0526, USA*

Communicated by J. Lega

Abstract

Collisions and interactions of dispersive shock waves in defocusing (repulsive) nonlinear Schrödinger type systems are investigated analytically and numerically. Two canonical cases are considered. In one case, two counterpropagating dispersive shock waves experience a head-on collision, interact and eventually exit the interaction region with larger amplitudes and altered speeds. In the other case, a fast dispersive shock overtakes a slower one, giving rise to an interaction. Eventually the two merge into a single dispersive shock wave. In both cases, the interaction region is described by a modulated, quasi-periodic two-phase solution of the nonlinear Schrödinger equation. The boundaries between the background density, dispersive shock waves and their interaction region are calculated by solving the Whitham modulation equations. These asymptotic results are in excellent agreement with full numerical simulations. It is further shown that the interactions of two dispersive shock waves have some qualitative similarities to the interactions of two classical shock waves.
© 2007 Elsevier B.V. All rights reserved.

1. Introduction

Shock waves in hydrodynamic systems, where the dominant regularization mechanism is small dispersion (as opposed to small dissipation in the classical, viscous case), have been realized experimentally in many diverse systems including plasmas [1], water waves [2], and more recently Bose–Einstein condensates [3,4] and nonlinear optics [5]. Individual dispersive shock waves (DSWs), characterized by expanding, modulated, periodic 1-phase waves, have been well-studied theoretically [6–9,4]; a detailed understanding of multiphase waves and DSW interactions in particular, is still lacking. In this work, we present a theory of dispersive shock wave interactions.

Although DSW interactions can be quite complicated, we show in this work that, for large time, asymptotically they are analogous to the interaction of two classical, viscous shock waves (VSWs) with an interaction region described by modu-lated quasiperiodic waves. This agrees with, but goes much further than, the discussion in [4] where it was shown that a single DSW is directly comparable (shape and speed) to a VSW when viewed in an averaged sense. Shock waves in dissipative gas dynamics are understood by invoking jump and entropy conditions across a shock front (see e.g. [10–12]). Although a very different regularization method – Whitham averaging – is used for dispersive shock waves, we show that the qualitative features of DSWs and their interactions are similar to the viscous case. Note that recent experiments in the field of nonlinear optics have observed interactions in dispersive shock waves [5].

Dispersive shock waves are described by slowly modulated periodic 1-phase waves [6,7]. The modulation equations describing the slow evolution of the waves are known as the Whitham equations. Whitham derived these equations by making an adiabatic assumption on the wave's parameters and averaging the governing equation's conservation laws over a period of oscillation [13]. To asymptotically describe the slowly modulated wave, one must solve the Whitham equations with appropriate initial data and boundary conditions.

---

* Corresponding author. Tel.: +1 303 497 4282.
 E-mail address: hoefer@boulder.nist.gov (M.A. Hoefer).

Slowly varying multiphase waves are considerably more complicated. The first discussion of general multiphase waves goes back to 1970 [14]; the multiphase Whitham equations for integrable systems were developed for the Korteweg–deVries (KdV) equation in [15] and for the nonlinear Schrödinger equation (NLS) in [16]. The theory to analyse these equations in the context of piecewise constant initial data, the type we consider in this work, was advanced by Kodama [17] and Biondini, Kodama [18]. An appropriate choice of initial data for the Whitham equations results in a global, rarefaction type solution. This procedure is termed *initial data regularization*. Matching of boundary data between 0 and 1-phase regions was carried out for modulated 1-phase waves in, for example, [6,7, 19,8,9].

Initial data regularization was first introduced in [17] and used in the analysis of nonreturn-to-zero optical communications formats. Later in [18], it was employed in the investigation of a particular class of multiphase interactions useful in the generation of ultrashort optical pulses and then in [4] it was used to analyse a single DSW in KdV and NLS systems. In this paper, we use this method to analyse the interaction of two DSWs. We consider two types of interactions: counterpropagating collisions and unidirectional merging. In the former, two DSWs propagate toward one another, collide, interact, and emerge with larger amplitudes and altered speeds. In the latter, one DSW overtakes another DSW, interaction ensues and results in the eventual merger of the two dispersive shocks. We show that modulated 2-phase or quasiperiodic solutions describe the interaction region. Moreover, for a certain choice of initial data, a 2-phase interaction region remains for all finite times but becomes degenerate as $t \to \infty$.

The outline of this article is as follows. In Section 2 we introduce the relevant asymptotic equations, the Whitham modulation equations. Because the 2-*phase* Whitham equations contain nontrivial hyperelliptical integrals, we introduce a numerical method to evaluate these integrals in Section 3. In Section 4, we discuss the dispersive regularization of shock waves. The main results in this article are presented in Section 5 where the Whitham modulation equations are solved for both counterpropagating, colliding DSWs and copropagating, merging DSWs. Complete bifurcation diagrams for these interaction processes are determined from these solutions. The boundaries separating different phase regions in the bifurcation diagrams are shown to compare quantitatively with numerical simulation of the NLS equation. In Section 6, we solve the analogous interaction problems for VSWs, and show that their long time behaviour is often qualitatively similar to the dispersively regularized shock problems.

2. Model equations

The defocusing NLS equation in a nondimensional form useful for our purposes is

$$i \varepsilon \Psi_t = -\frac{\varepsilon^2}{2} \Psi_{xx} + |\Psi|^2 \Psi. \tag{1}$$

We are interested in the case $0 < \varepsilon \ll 1$, corresponding to small dispersion. This asymptotic regime is the semiclassical limit referring to a quantum mechanical interpretation where Planck's constant is vanishingly small; $\hbar \to 0$. This equation models the wavefunction of a repulsive Bose–Einstein condensate (BEC) in free expansion when a dimensional reduction is applied [20]. The case $0 < \varepsilon \ll 1$ corresponds to the strong interaction regime. The slowly varying envelope of the electromagnetic field propagating in a Kerr material is also modeled by the NLS equation (1), where time t is replaced by the propagation direction and the dispersive term corresponds to diffraction in the material [21]. The case $0 < \varepsilon \ll 1$ corresponds to strong nonlinearity hence a large laser intensity. Recent experiments in both of these systems have demonstrated the existence of DSWs [3–5].

2.1. Hydrodynamic form

The NLS equation (1) can also be represented in a form analogous to the Euler equations of gas dynamics. The transformation

$$\Psi(x, t) = \sqrt{\rho(x, t)} e^{\frac{i}{\varepsilon} \int_0^x u(x', t) \, dx'},$$

along with the first two local conservation laws for the NLS equation give [22]

$$\rho_t + (\rho u)_x = 0$$
$$(\rho u)_t + \left(\rho u^2 + \frac{1}{2} \rho^2 \right)_x = \frac{\varepsilon^2}{4} (\rho (\log \rho)_{xx})_x. \tag{2}$$

When $\varepsilon = 0$, these equations are known as the compressible Euler equations for a perfect, isentropic gas with fluid density ρ, local fluid velocity u, and adiabatic constant $\gamma = 2$. The equations are also known as the shallow water equations with fluid height ρ and local fluid velocity u. It is well known that the Euler equations admit solutions that develop an infinite derivative in finite time, shock waves. In the context of classical viscous gas dynamics, these solutions are regularized by adding a small amount of dissipation to the equation or, equivalently, invoking jump conditions across an entropy satisfying discontinuity [11].

Because the term in Eqs. (2) multiplied by ε^2 is derived from the dispersive term $\frac{\varepsilon^2}{2} \Psi_{xx}$ in Eq. (1), we refer to it as a dispersive term. When a steep gradient forms, the solution develops oscillations with wavelength of $O(\varepsilon)$. In general, the $\varepsilon \to 0$ limit is a weak limit and is described by the Whitham modulation equations [16]. The required number of modulation equations corresponds to the number of phases, which, in turn, corresponds to the complexity in the underlying (slowly varying) quasi-periodic solution. Since we will require modulated 2-phase solutions to describe DSW interactions, we now outline the first three sets of equations in the NLS-Whitham hierarchy.

2.2. Euler equations: 0-phase solutions

When there is no shock formation in Eqs. (2), the $\varepsilon \to 0$ limit is accurately described by solutions of the Euler equations.

We consider only simple slowly varying periodic solutions to Eqs. (2) with $\varepsilon \to 0$, or, equivalently, the solution

$$\Psi_0(x, t, \theta_0) = \sqrt{\omega_0 - \kappa_0^2} e^{i\theta_0}, \quad \frac{\partial \theta_0}{\partial x} = \kappa_0/\varepsilon,$$

$$\frac{\partial \theta_0}{\partial t} = -\omega_0/\varepsilon, \tag{3}$$

to Eq. (1). Then the density and velocity are

$$\rho(x, t) = |\omega_0 - \kappa_0^2|, \quad u(x, t) = \kappa_0,$$

with κ_0 and ω_0 slowly varying. Here and throughout this work, x and t are slow variables. The phase θ_0 is a fast variable. We refer to these solutions as 0-*phase*. The Euler equations may be conveniently written in Riemann invariant form [12]

$$\frac{\partial r_+}{\partial t} + v_+ \frac{\partial r_+}{\partial x} = 0,$$

$$\frac{\partial r_-}{\partial t} + v_- \frac{\partial r_-}{\partial x} = 0, \tag{4}$$

$$r_+ = u + 2\sqrt{\rho}, \quad r_- = u - 2\sqrt{\rho},$$

$$v_+(r_-, r_+) = \frac{1}{4}(3r_+ + r_-), \quad v_-(r_-, r_+) = \frac{1}{4}(r_+ + 3r_-).$$

A solution to Eqs. (2) with $0 < \varepsilon \ll 1$ that is accurately approximated by the asymptotic solution (3) and 0-phase equations (4) (i.e. there is no breaking) is deemed a 0-*phase* solution.

2.3. 1-phase solutions

When a single, isolated dispersive shock forms (e.g. in the case of an initial step), it is described asymptotically by a modulated periodic or 1-*phase* solution of Eqs. (2) [7]

$$\rho(x, t, \theta) = \lambda_3(x, t) - (\lambda_3(x, t) - \lambda_1(x, t))dn^2(\theta; m(x, t)),$$

$$u(x, t; \varepsilon) = V(x, t) - \sigma(x, t)\frac{\sqrt{\lambda_1(x, t)\lambda_2(x, t)\lambda_3(x, t)}}{\rho(x, t, \theta)},$$

$$m(x, t) = \frac{\lambda_2(x, t) - \lambda_1(x, t)}{\lambda_3(x, t) - \lambda_1(x, t)}, \quad \sigma(x, t) = \pm 1, \tag{5}$$

$$\frac{\partial \theta}{\partial x} = \sqrt{\lambda_3(x, t) - \lambda_1(x, t)}/\varepsilon,$$

$$\frac{\partial \theta}{\partial t} = -V(x, t)\sqrt{\lambda_3(x, t) - \lambda_1(x, t)}/\varepsilon,$$

where we have written the solution in terms of the slow variables x, t, and the fast phase θ. Equivalently, we can write this as a slowly varying complex valued solution to Eq. (1) as

$$\Psi_1(x, t, \theta_0, \theta_1) = f(\theta_1)e^{i\theta_0}, \quad \frac{\partial \theta_i}{\partial x} = \kappa_i(x, t)/\varepsilon,$$

$$\frac{\partial \theta_i}{\partial t} = -\omega_i(x, t)/\varepsilon, \quad i = 0, 1, \tag{6}$$

for appropriate f, κ_i and ω_i, $i = 1, 2$, given in terms of λ_i, $i = 1, 2, 3$ and V. The elliptic function solution Eq. (5) has four parameters: $\lambda_1, \lambda_2, \lambda_3$, and V. The $\varepsilon \to 0$ limit is achieved by considering slow parameter modulations of the fast oscillatory

solution. Equations describing the evolution of these parameters are the Whitham 1-*phase* equations [23,7],

$$\frac{\partial r_i}{\partial t} + v_i^{(1)}(\vec{r})\frac{\partial r_i}{\partial x} = 0, \quad i = 1, 2, 3, 4. \tag{7a}$$

These equations are a system of first order, quasilinear, hyperbolic equations in Riemann invariant form [17]. The 1-phase velocities $v_i^{(1)}$ are expressions involving complete first, $K(m)$, and second, $E(m)$, elliptical integrals:

$$v_1^{(1)}(r_1, r_2, r_3, r_4) = V - \frac{1}{2}(r_2 - r_1)$$
$$\times \left[1 - \frac{(r_4 - r_2)E(m)}{(r_4 - r_1)K(m)} \right]^{-1},$$

$$v_2^{(1)}(r_1, r_2, r_3, r_4) = V + \frac{1}{2}(r_2 - r_1)$$
$$\times \left[1 - \frac{(r_3 - r_1)E(m)}{(r_3 - r_2)K(m)} \right]^{-1},$$

$$v_3^{(1)}(r_1, r_2, r_3, r_4) = V - \frac{1}{2}(r_4 - r_3) \tag{7b}$$
$$\times \left[1 - \frac{(r_4 - r_2)E(m)}{(r_3 - r_2)K(m)} \right]^{-1},$$

$$v_4^{(1)}(r_1, r_2, r_3, r_4) = V + \frac{1}{2}(r_4 - r_3)$$
$$\times \left[1 - \frac{(r_3 - r_1)E(m)}{(r_4 - r_1)K(m)} \right]^{-1},$$

$$m(r_1, r_2, r_3, r_4) = \frac{(r_4 - r_3)(r_2 - r_1)}{(r_4 - r_2)(r_3 - r_1)}.$$

The original solution parameters in Eq. (5) are expressed in terms of the 1-phase Riemann invariants r_i:

$$\lambda_1 = \frac{1}{16}(r_1 - r_2 - r_3 + r_4)^2,$$

$$\lambda_2 = \frac{1}{16}(-r_1 + r_2 - r_3 + r_4)^2,$$

$$\lambda_3 = \frac{1}{16}(-r_1 - r_2 + r_3 + r_4)^2, \tag{8}$$

$$V = \frac{1}{4}(r_1 + r_2 + r_3 + r_4), r_1 < r_2 < r_3 < r_4.$$

Given the solution to the Whitham equations (7), the asymptotic solution (5) is reconstructed by using Eqs. (8) and integrating the phase θ in Eq. (5) appropriately. We take

$$\theta(x, t) = \frac{1}{\varepsilon} \left[\int_{x_0}^{x} \sqrt{\lambda_3(x', t) - \lambda_1(x', t)} \, dx' \right.$$
$$\left. - \int_0^t V(x_0, t')\sqrt{\lambda_3(x_0, t') - \lambda_1(x_0, t')} \, dt' \right] + \theta_0,$$

where θ_0 is the initial phase at $x = x_0, t = 0$.

A solution to Eqs. (2) with $0 < \varepsilon \ll 1$ that is accurately approximated by the asymptotic solution Eq. (6) and 1-phase equations (7) but not the Euler equations (i.e. the 0-phase equations (4)), is deemed a 1-*phase* solution.
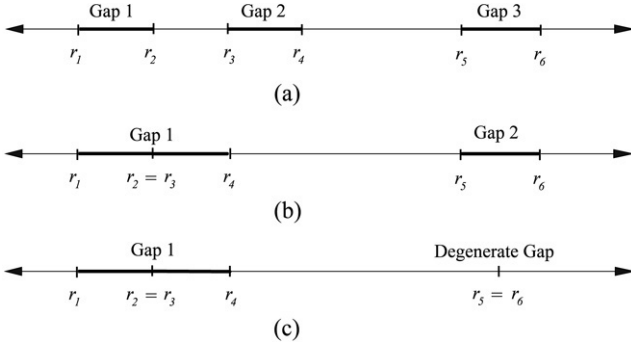
Fig. 1. (a) Three gaps in the spectrum of the linear operator (10) associated with the NLS equation. To accurately represent the spectrum, six gap edges r_i are required. These gap edges correspond to six parameters in a 2-*phase* solution Ψ_2 (9) of the NLS equation. (b) A degenerate gap forms when two gap edges are equal $r_2 = r_3$. The spectrum is now represented by four gap edges r_1, r_4, r_5, r_6, corresponding to four parameters in a 1-*phase* solution Ψ_1 (6) of the NLS equation. (c) Now two gaps are degenerate, leaving only one gap and two gap edges r_1 and r_4, which correspond to parameters in a 0-*phase* solution Ψ_0 (3) of the NLS equation.

2.4. 2-phase solutions

The 1-phase solution (5) may be generalized to N-phase solutions of the NLS equation with the help of the periodic/quasi-periodic inverse scattering technique [24]. In this work, we are interested in 2-*phase* solutions. This solution is written in the form

$$
\Psi_2(x, t, \theta_0, \theta_1, \theta_2) = f(\theta_1, \theta_2)e^{i\theta_0},
$$
$$
\frac{\partial \theta_i}{\partial x} = \kappa_i(x, t)/\varepsilon, \qquad \frac{\partial \theta_i}{\partial t} = -\omega_i(x, t)/\varepsilon, \tag{9}
$$
$$
i = 0, 1, 2,
$$

where f is 2π periodic in each phase θ_i, $i = 0, 1, 2$, and is represented in terms of multidimensional theta functions [24]. The phases θ_i are fast variables with six independent parameters: the wavenumbers κ_i, $i = 0, 1, 2$, and the frequencies ω_i, $i = 0, 1, 2$, that are allowed to vary slowly in space and time. Applying Floquet theory on the self-adjoint linear operator associated with the NLS equation [25,16],

$$
L = \begin{pmatrix} i\varepsilon\partial_x & -i\,\Psi_2 \\ i\,\Psi_2^* & -i\varepsilon\partial_x \end{pmatrix}, \tag{10}
$$

shows that its spectrum consists of closed intervals on the real axis

$$
(-\infty, r_1] \cup [r_2, r_3] \cup [r_4, r_5] \cup [r_6, \infty),
$$

separated by up to three gaps with endpoints $\{r_i\}_{i=1}^6$ called the simple eigenvalues. As Fig. 1 shows, when two endpoints coincide, a degeneracy occurs and there is one less gap. The gap endpoints are directly related to the wavenumbers and frequencies in the phases θ_i and are the Riemann invariants for the modulation equations [24].

The NLS equation has an infinite number of conservation laws. We require six to describe the slow modulations of the six parameters r_i. Averaging of six conservation laws over the fast phases θ_i gives the Whitham modulation equations [16,23,18]

$$
\frac{\partial r_i}{\partial t} + v_i^{(2)}(\vec{r})\frac{\partial r_i}{\partial x} = 0, \quad i = 1, 2, \ldots, 6. \tag{11a}
$$

The Whitham velocities are given in terms of hyperelliptic integrals,

$$
v_i^{(2)}(\vec{r}) = \frac{r_i^4 - \frac{1}{2}\sigma_1 r_i^3 + \frac{1}{2}(\sigma_2 - \frac{1}{4}\sigma_1^2)r_i^2 + \gamma_1 r_i + \gamma_2}{r_i^3 - \frac{1}{2}\sigma_1 r_i^2 + \alpha_1 r_i + \alpha_2}, \tag{11b}
$$

$$
\sigma_1 = \sum_{k=1}^{6} r_k, \quad \sigma_2 = \sum_{j=1}^{5}\sum_{k=j+1}^{6} r_j r_k. \tag{11c}
$$

The coefficients γ_1, γ_2, α_1, and α_2 are solutions to the following linear systems

$$
\begin{bmatrix} I_1^1 & I_1^0 \\ I_2^1 & I_2^0 \end{bmatrix}\begin{bmatrix} \alpha_1 \\ \alpha_2 \end{bmatrix} = \begin{bmatrix} \frac{1}{2}\sigma_1 I_1^2 - I_1^3 \\ \frac{1}{2}\sigma_1 I_2^2 - I_2^3 \end{bmatrix}, \tag{11d}
$$

$$
\begin{bmatrix} I_1^1 & I_1^0 \\ I_2^1 & I_2^0 \end{bmatrix}\begin{bmatrix} \gamma_1 \\ \gamma_2 \end{bmatrix} = \begin{bmatrix} -\frac{1}{2}\left(\sigma_2 - \frac{1}{4}\sigma_1^2\right)I_1^2 + \frac{1}{2}\sigma_1 I_1^3 - I_1^4 \\ -\frac{1}{2}\left(\sigma_2 - \frac{1}{4}\sigma_1^2\right)I_2^2 + \frac{1}{2}\sigma_1 I_2^3 - I_2^4 \end{bmatrix}. \tag{11e}
$$

The I_j^k are hyperelliptic integrals

$$
I_j^k = \frac{1}{2}\int_{r_{2j+1}}^{r_{2j+2}} \frac{z^k}{\sqrt{-\prod_{l=1}^{6}(z - r_l)}}\,\mathrm{d}z. \tag{12}
$$

A solution to Eqs. (2) with $0 < \varepsilon \ll 1$ that is accurately approximated by the asymptotic solution (9) and the 2-phase Eqs. (11) but not Eqs. (7) or (4) is a 2-*phase* solution.

2.4.1. Symmetry in the 2-phase Whitham equations

The 2-phase velocities $v_i^{(2)}$ exhibit the following symmetry:

$$
\begin{aligned}
&v_i^{(2)}(r_1, r_2, r_3, r_4, r_5, r_6) \\
&= -v_{7-i}^{(2)}(-r_6, -r_5, -r_4, -r_3, -r_2, -r_1), \tag{13}
\end{aligned}
$$

for $i = 1, 2, \ldots, 6$. To prove this result, we start by noting that there are certain symmetries for the coefficients in Eq. (11b)

$$
\begin{aligned}
&\alpha_k(-r_6, \ldots, -r_1) = (-1)^{k+1}\alpha_k(r_1, \ldots, r_6), \\
&\gamma_k(-r_6, \ldots, -r_1) = (-1)^k\gamma_k(r_1, \ldots, r_6), \\
&\sigma_j(-r_6, \ldots, -r_1) = (-1)^j\sigma_j(r_1, \ldots, r_6), \\
&k = 1, 2, \ldots, 6, \quad j = 1, 2. \tag{14}
\end{aligned}
$$

The symmetry for the σ_j can be calculated directly from Eqs. (11c). The defining equations for the α_k and γ_k (Eqs. (11d) and (11e)) result from equating to zero the integrals of certain meromorphic (Abelian) differentials over *any* linearly independent set of two a-cycles on the Riemann surface [16,23]

$$
\mu^2(\lambda) = \prod_{k=1}^{6}(\lambda - r_k).
$$

By a change of variable, one can show that the defining equations for both $\alpha_k(r_1, \ldots, r_6)$ and $(-1)^{k+1}\alpha_k(-r_6, \ldots, -r_1)$ are equivalent. Similarly, the defining equations for $\gamma_k(r_1, \ldots, r_6)$ and $(-1)^k \gamma_k(-r_6, \ldots, -r_1)$ are equivalent. By uniqueness of solutions to the linear equations (11d) and (11e), the symmetries (14) must hold. The symmetries in the coefficients (14) are then used to show the symmetry for the velocities in Eq. (13) by direct calculation. A corollary of the symmetry (13) is that if the initial data satisfy

$$r_6(x, 0) = -r_1(-x, 0), \quad r_5(x, 0) = -r_2(-x, 0),$$
$$r_4(x, 0) = -r_3(-x, 0), \tag{15}$$

then Eqs. (11a) are satisfied, and existence/uniqueness establishes that this symmetry $(r_{7-i}(x, t) = -r_i(-x, t), i = 1, 2, \ldots, 6)$ is maintained for all time. This will be useful in our analysis of DSW collisions.

The result in Eq. (13) can be generalized to the N-phase case by the same argument

$$v_i^{(N)}(r_1, r_2, \ldots, r_{2N+2})$$
$$= -v_{2N+3-i}^{(N)}(-r_{2N+2}, -r_{2N+1}, \ldots, -r_1),$$

for $i = 1, 2, \ldots, 2N + 2$.

In summary, there exist asymptotic solutions of the NLS equation (1) described by slow modulations of the Euler (0-phase), 1, or 2-phase solutions. The number of phases in the solution corresponds directly to the number of gaps in the spectrum of the linear operator (10) (see Fig. 1). It is therefore possible that a solution is described locally by a modulated 2-phase solution (when each r_i is distinct) but degenerates to a 1-phase or 0-phase solution if pairs of the r_i merge at some other location in space or time. As we will show, this is the case when two dispersive shock waves interact.

Perturbation theory indicates that the Whitham equations are valid for times $t \ll 1/\varepsilon$ which is consistent with what we obtain here. Improving the description for longer times, e.g. $t = O(1/\varepsilon)$, or a detailed error analysis are outside the scope of this paper.

3. Numerical evaluation of hyperelliptical integrals

The Whitham equations (11) involve hyperelliptic integrals. Closed-form analytical expressions for hyperelliptic integrals exist only in highly symmetrical cases [26]. Because we must evaluate the velocities $v_i^{(2)}$, we present an efficient numerical method to evaluate these integrals based on a Chebyshev technique presented in [27].

Transformation of variables $z = c_j t + d_j$ in Eq. (12) reduces it to

$$I_j^k = \int_{-1}^1 \frac{(c_j t + d_j)^k}{\sqrt{1 - t^2}} H_j(t)\, \mathrm{d}t,$$
$$c_j = \frac{1}{2}(r_{2j+2} - r_{2j+1}), \quad d_j = \frac{1}{2}(r_{2j+2} + r_{2j+1}),$$
$$H_j(t) = \frac{1}{2}\left[\prod_{\substack{l=1 \\ l \neq 2j+1, 2j+2}}^{6} (c_j t + d_j - r_l) \right]^{-1/2}.$$

Define the weighted inner product

$$\langle f, g \rangle = \int_{-1}^1 \frac{f(t)g(t)}{\sqrt{1 - t^2}}\, \mathrm{d}t. \tag{16}$$

Linearity of this inner product and the binomial expansion imply

$$I_j^k = \left\langle \sum_{l=0}^k \binom{k}{l} c_j^l d_j^{k-l} t^l, H_j(t) \right\rangle$$
$$= \sum_{l=0}^k \binom{k}{l} c_j^l d_j^{k-l} \langle t^l, H_j(t) \rangle.$$

Since the Chebyshev polynomials $T_n(t) \equiv \cos^{-1}(n\cos(t))$ are orthogonal with respect to the inner product equation (16), we expand the monomials t^l in terms of them

$$t^l = \sum_{n=0}^l b_n^{(l)} T_n(t).$$

Expanding the function $H_j(t)$ in an infinite series of Chebyshev polynomials gives

$$H_j(t) = \sum_{i=0}^{\infty} a_i^{(j)} T_i(t). \tag{17}$$

Due to orthogonality of the T_n, we have

$$I_j^k = \sum_{l=0}^k \binom{k}{l} c_j^l d_j^{k-l} \sum_{n=0}^l b_n^{(l)} \langle T_n, H_j \rangle$$
$$= \sum_{l=0}^k \binom{k}{l} c_j^l d_j^{k-l} \sum_{n=0}^l b_n^{(l)} \frac{\pi}{2} e_n a_n^{(j)},$$
$$e_n = \begin{cases} 2 & n = 0 \\ 1 & n > 0. \end{cases}$$

We have converted the evaluation of the hyperelliptic integrals, Eqs. (12), to a finite linear combination of the Chebyshev coefficients of $H_j(t)$. In practice, the infinite expansion (17) must be truncated at a finite number of terms N, where

$$H_j(t) \approx \sum_{i=0}^N a_i^{(j)}(N) T_i(t). \tag{18}$$

The coefficients $a_n^{(j)}(N)$ are found by use of a fast discrete cosine transform [28].

To determine the accuracy of this method, we evaluated the integrals I_1^{2k} for $k = 0, 1, 2$ for different choices of the Riemann invariants $\{r_i\}$. The integrals I_1^{2k} can be evaluated explicitly in terms of elliptic functions of the first, second and third kinds for the special case

$$r_1 = -2, \quad r_2 = r_3 - \nu, \quad r_3 = 1,$$
$$r_4 = -r_3, \quad r_5 = -r_2, \quad r_6 = -r_1, \tag{19}$$

where $0 < \nu < 1$ (see [26]). We choose ν to be small because $\nu = 0$ corresponds to the coincidence of r_2 and r_3, which is what occurs in a degenerate gap in the spectrum of (10).
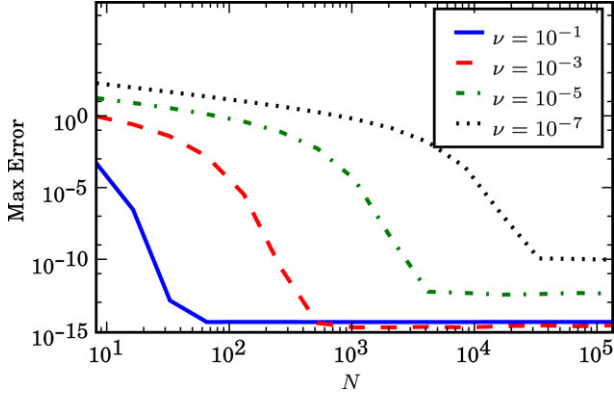
Fig. 2. Error in numerical method for hyperelliptical integral evaluation as a function of N, the number of Chebyshev polynomials used in the expansion of $H_j(t)$ in Eq. (18). The different error curves correspond to different values for gap separation $r_3 - r_2 = \nu$ in Eqs. (19).

The choice $0 < \nu \ll 1$ also tests the stability/accuracy of the numerical method. Fig. 2 is a log–log plot of the error as a function of N, the number of Chebyshev polynomials used in the expansion (18), for several ν. As the figure shows, this numerical method gives spectral convergence of the integrals of interest. The flattening of the error larger than machine precision for the smaller values of ν is due most likely to numerical errors in the evaluation of the first, second, and third elliptic integrals in the numerical package SciPy [29], the Python programming language's computational library, not to any inherent limitations in our method.

In all of our evaluations of hyperelliptic integrals, we use a refinement technique as follows. We compute $a_i^{(j)}(N)$ and $a_i^{(j)}(2N)$ for $N = 2^3, 2^4, \ldots$ until their difference is less than an absolute tolerance of 10^{-12}. Typically, $N = 64$ terms are required with a maximum of $N = 2^{17}$ for certain degenerate gaps, the smallest of which we consider are $r_{i+1} - r_i = 2 \times 10^{-7}$.

4. Dispersive regularization

As shown in [17,18,4], the dispersive regularization of the conservation laws (2) with piecewise constant initial data can be formulated as follows. If the initial data are nondecreasing, there is no breaking. In this case the (leading order) dissipative and dispersive regularizations are the same. The asymptotic solution admits a 0-phase representation, and so one solves the 0-phase equations (4). If the initial data are decreasing, then the number of phases in the asymptotic solution must be increased. Hence the number of modulation parameters (Riemann invariants) $\{r_i\}_{i=1}^N$ must be expanded so as to satisfy the following three properties:

$$
\begin{aligned}
\overline{\rho}(x,0) &= \rho(x,0;\varepsilon) \\
\overline{u}(x,0) &= u(x,0;\varepsilon)
\end{aligned}
\quad \text{(characterization)},
$$

$$
r_i(x,0) \leq r_i(y,0) \quad \text{if } x < y \quad \text{(non-decreasing)}, \tag{20}
$$

$$
\max_{x \in \mathbb{R}} r_i(x,0) < \min_{x \in \mathbb{R}} r_{i+1}(x,0) \quad \text{(separability)}.
$$

The expressions $\overline{\rho}$ and $\overline{u}$ are the averages of the asymptotic N-phase solution over the fast phases. For example, the 1-phase
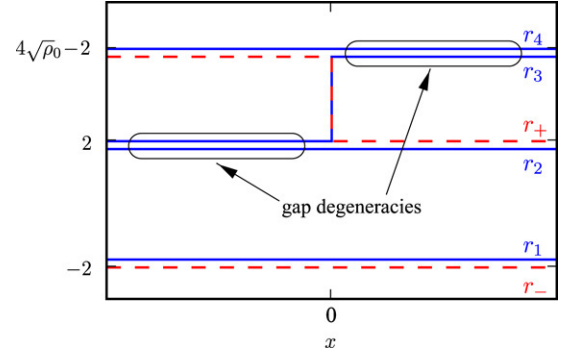
Fig. 3. Initial data regularization for a single shock initial condition ($\rho(x,0) = \rho_0$ and $u(x,0) = 2\sqrt{\rho_0} - 2$ when $x < 0$; $\rho(x,0) = 1$ and $u(x,0) = 0$ for $x > 0$). Overlapping of the initial data for pairs of Riemann invariants correspond to gap degeneracies hence "cancel out".

average of the density in Eq. (5) is

$$
\overline{\rho}(x,t) = \frac{1}{L} \int_0^L \rho(x,t,\theta) \, d\theta = \lambda_3 - (\lambda_3 - \lambda_1) \frac{E(m)}{K(m)},
$$
$$
L = 2K(m).
$$

We take the minimum number of Riemann invariants that satisfy the above properties. When these properties hold, a global, rarefaction type solution exists. The separability condition is a sufficient, but not necessary, condition, as we will show in two examples. A necessary condition is that the Riemann invariants must not cross. Sometimes we can only satisfy the first two conditions in (20) but nevertheless find a global solution to the Whitham equations.

Initial data for the Riemann invariants must be chosen so that, when inserted into the 0, 1, or 2-phase modulated solution and compared with the initial data for the originally formulated problem, the two agree. This is the *characterization* property in (20). In practice, this regularization procedure is performed by utilizing degeneracies in the spectrum of (10) whereby the initial data for the 0-phase Riemann invariants is "matched" to the initial data of higher phase Riemann invariants. We explain this procedure with an example.

The regularization for a single shock initial condition is shown in Fig. 3. In this example, the 1-phase Riemann invariants $\{r_i\}_{i=1}^4$ (solid) satisfy conditions (20) but the 0-phase invariants (dashed) do not (one of them is decreasing). The nondecreasing and separability conditions for the 1-phase Riemann invariants are clear from Fig. 3. The characterization property can be directly verified by inserting the values for the r_i's into Eqs. (8) and (5) and taking the sign σ in Eq. (5) to be (see [19,4] for a complete discussion of the choice of σ, which is due to the nonexistence/existence of a vacuum point in the asymptotic solution)

$$
\sigma(x,0) = \begin{cases} 1 & 1 < \rho_0 < 4 \\ \text{sgn}(x) & 4 < \rho_0. \end{cases}
$$

Then the initial data in Fig. 3 corresponds exactly to an initial step in ρ and u. Therefore, a single shock is described by the modulated 1-phase solution (5).

Another, simpler way to verify the characterization property is to note the following. Wherever two Riemann invariants

of the same class (1-phase in this case) overlap, they are degenerate (see Fig. 1). In this case, we have a reduction of g gaps to $g - 1$ gaps. Hence the overlapping Riemann invariants can be considered to "cancel out" as a contribution to the initial data. For step initial data, the 0-phase Riemann invariants *must* coincide exactly with the initial data for a *single* 1-phase Riemann invariant. If the 0-phase initial data can be made to coincide with a single 1-phase Riemann invariant at each point in space *and* all other values of the 1-phase Riemann invariants that do not coincide with 0-phase initial data "cancel out", then the initial data are properly characterized. More details of this regularization procedure can be found in [17,18,4].

The same method generalizes when performing a 2-phase regularization of the type of initial data we will consider in this work.

In Ref. [11], Lax showed that a system of two hyperbolic equations

$$\frac{\partial r_i}{\partial t} + v_i(r_1, r_2)\frac{\partial r_i}{\partial x} = 0, \quad i = 1, 2, \tag{21}$$

has a global solution, provided that

$$\frac{\partial v_i}{\partial r_i} > 0, \tag{22}$$

and that the initial data are nondecreasing

$$r_i(x, 0) \leq r_i(y, 0) \quad \text{if } x < y. \tag{23}$$

The condition (22) was shown to hold for the NLS Whitham equations (11) in [17]. The condition (23) coupled with the ordering condition,

$$\max_{x \in \mathbb{R}} r_1(x, 0) < \min_{x \in \mathbb{R}} r_2(x, 0),$$

proves that a nonintersecting rarefaction type solution to Eqs. (21) exists for all time. Since at most two of the six Riemann invariants in the 2-phase Whitham equations (11) will locally vary in our analysis, the above is a proof of initial data regularization for the case of DSW interactions.

A useful result when calculating the solutions to the Whitham equations (4), (7) and (11) is the following speed ordering proved in [17]

$$r_i < r_j \Rightarrow v_i^{(k)} < v_j^{(k)}, \tag{24}$$

for $k = 0$, $i \equiv -$ and $j \equiv +$; for $k = 1$, $1 \leq i < j \leq 4$; for $k = 2$, $1 \leq i < j \leq 6$.

5. DSW interaction

We now consider solutions of the NLS equation (1) or equivalently, the dispersive hydrodynamic equations (2), for two shock initial data. Two cases are of interest. The first corresponds to the situation where two DSWs are propagating toward one another, resulting in a collision. The second case is when a fast DSW overtakes a slower one, a situation we call merging.
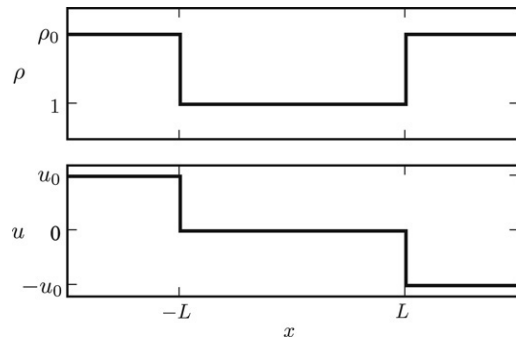
Fig. 4. Initial data for two shock collision.

5.1. Collision

The case of two DSWs propagating toward each other gives rise to a collision. In this section, we investigate the nature of the collision process. The relevant initial data for Eqs. (2) are (see also Fig. 4)

$$\rho(x, 0) = \begin{cases} \rho_0 & |x| > L \\ 1 & |x| < L, \end{cases}$$

$$u(x, 0) = \begin{cases} -\text{sgn}(x)u_0 & |x| > L \\ 0 & |x| < L, \end{cases} \tag{25}$$

where $\rho_0 > 1$. This initial data can be generalized with the rescaling

$$\tilde{\rho} = \rho_m\rho, \quad \tilde{u} = \sqrt{\rho_m}u + u_m, \quad t = \rho_m\tilde{t},$$
$$x = \sqrt{\rho_m}(\tilde{x} - u_m\tilde{t}), \quad \rho_m > 0, \tag{26}$$

which leaves Eq. (2) invariant. Then the initial data (25) in the scaled coordinate system (26) takes the form

$$\tilde{\rho}(\tilde{x}, 0) = \begin{cases} \rho_{\text{out}} & |\tilde{x}| > \tilde{L} \\ \rho_m & |\tilde{x}| < \tilde{L}, \end{cases}$$

$$\tilde{u}(\tilde{x}, 0) = \begin{cases} -\text{sgn}(\tilde{x})u_{\text{out}} & |\tilde{x}| > \tilde{L} \\ u_m & |\tilde{x}| < \tilde{L}, \end{cases}$$

where $\rho_{\text{out}} = \rho_m\rho_0$, $u_{\text{out}} = \sqrt{\rho_m}u_0 + u_m$, $\tilde{L} = L/\sqrt{\rho_m}$, $\rho_m > 0$ and u_m arbitrary. The velocities, $\tilde{v}$, in this scaled coordinate system are related to the velocities, v, we calculate in this work by

$$\tilde{v} = \sqrt{\rho_m}v + u_m.$$

Interaction behaviour depends on the value of u_0. By inserting the initial data (25) into the 0-phase Riemann invariants $r_\pm = u \pm 2\sqrt{\rho}$, we find six different values for them:

$$\{u_0 + 2\sqrt{\rho_0}, u_0 - 2\sqrt{\rho_0}, 2, -2, -u_0 + 2\sqrt{\rho_0}, -u_0 - 2\sqrt{\rho_0}\}.$$

The relative ordering of these values determines the interaction behaviour in the collision process. As we will show, this is because different orderings require different initial data regularizations. Fig. 5 depicts five different regions in u_0, ρ_0 space corresponding to qualitatively different types of interaction processes. The different regions correspond to different long time asymptotic states for the interaction. A summary of the results for each region is given in Section 5.1.7.
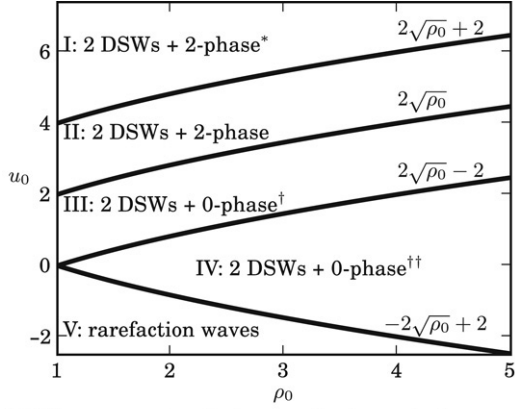
*DSWs connected to 2-phase region by periodic waves

†4 DSWs merge into 2 DSWs

††2 DSWs + 2 rarefaction waves merge into 2 DSWs

Fig. 5. Cases corresponding to different choices for the initial velocity u_0 as a function of the initial density ρ_0 in Eq. (25). There are five different regions that give qualitatively different results for the collision interaction. The long time, asymptotic state for each case is labelled. A summary of the collision process for each region is given in Section 5.1.7. A typical initial asymptotic solution for each region is shown in Fig. 6.

In general, a single initial step in ρ and u gives rise to two waves, a combination of DSWs and/or rarefaction waves [19]. Example *initial*, asymptotic ($0 < \varepsilon \ll 1$) behaviours for each region in Fig. 5 are depicted in Fig. 6. The asymptotic solutions were calculated by solving the 0 or 1-phase Whitham equations for the Riemann invariants, $r_\pm$ in the 0-phase case and r_i, $i = 1, 2, 3, 4$, in the 1-phase case. This solution was then inserted into either the 0-phase solution (3) or the 1-phase solution (5) with a finite value of ε ($\varepsilon = 0.02$ except where noted).

Two specific choices for the initial velocity u_0 are of particular physical interest and give rise to a simplified analysis. The simplest case is to assume a single shock at each step, which occurs when u_0 is taken at the boundaries between cases III and IV in Fig. 5. For this, we assume $u_0 = 2\sqrt{\rho_0} - 2$. To show that the results for this particular choice of u_0 apply with small modifications for other choices $-2\sqrt{\rho_0} + 2 < u_0 < 2\sqrt{\rho_0}$ corresponding to regions III and IV, we also consider the choice $u_0 = 0$, which has application to Bose–Einstein condensates. Finally, we consider cases I and II, because a novel *expanding* interaction region is generated.

Briefly, cases III and IV give rise to a 2-phase interaction region that eventually closes, leaving behind a constant, 0-phase region. The interaction of the DSWs in these cases ends in finite time and two counterpropagating DSWs remain. Cases I and II are different in that the 2-phase interaction region remains for all time, but one gap in the spectrum is asymptotically ($t \to \infty$) degenerate. Representative asymptotic 1-phase solutions corresponding to different regions in Fig. 5 *before* interaction occurs are shown in Fig. 6. We now explain these results in detail.

5.1.1. Initial data regularization: $u_0 = 2\sqrt{\rho_0} - 2$

Fig. 7 depicts the initial data (25) in terms of the 0-phase Riemann invariants $r_\pm = u \pm 2\sqrt{\rho}$ (dashed) and
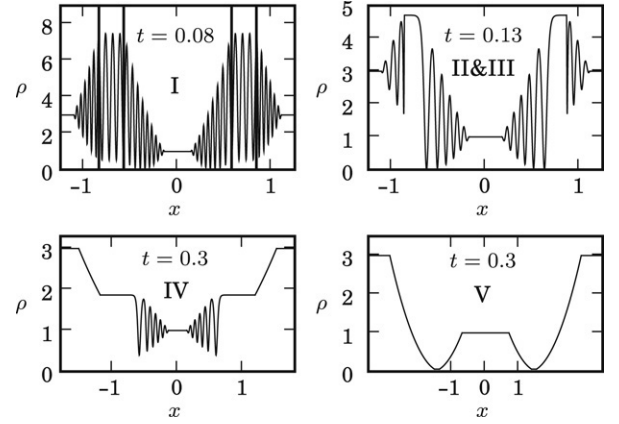
Fig. 6. Density ρ as a function of x in the asymptotic solution to the collision initial value problem *before* interaction occurs. Each labelled plot corresponds to a particular choice of ρ_0 and u_0 from a region of parameter space in Fig. 5. All plots assume $\rho_0 = 3$ and $L = 1$. The behaviour of the solution at each initial step is described as follows (see also [19]): I, upper left, $u_0 = 2\sqrt{\rho_0} + 4$: two DSWs connected by a pure 1-phase periodic region whose boundaries are delineated by vertical lines. II & III, upper right, $u_0 = 2\sqrt{\rho_0} - \frac{1}{4}$: two DSWs connected by a constant 0-phase region. Case IV, lower left, $u_0 = 0$: one rarefaction wave connected to a DSW by a constant 0-phase region. Case V, lower right, $u_0 = -2\sqrt{\rho_0} - 1$: two rarefaction waves connected by a constant 0-phase region. For the 1-phase results of cases I, II, and III, $\varepsilon = 0.075$, whereas for case IV, $\varepsilon = 0.035$. All the 0-phase results assume $\varepsilon = 0$.
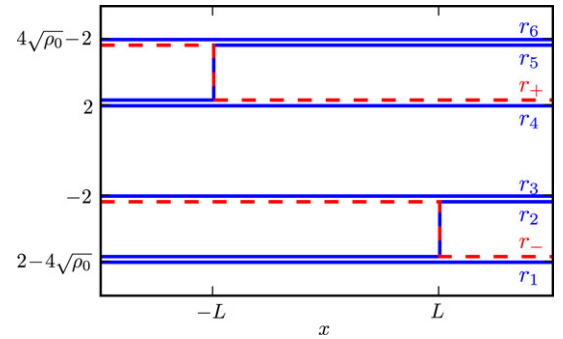
Fig. 7. Initial data for two pure DSWs propagating toward each other (r_- and r_+, dashed) and their regularization (r_i, solid).

its regularization in terms of the 2-phase Riemann invariants r_i, $i = 1, \ldots, 6$. The three properties, characterization, nondecreasing and separability of Eq. (20) are satisfied with this choice of initial data (see Section 4).

5.1.2. Solution of the Whitham equations: $u_0 = 2\sqrt{\rho_0} - 2$

In this section, we solve the 2-phase Whitham equations (11) for the initial data shown in Fig. 7. We take advantage of degeneracies whereby pairs of the Riemann invariants coincide. In these regions, the solution is described by a 0 or 1-phase solution, which is found analytically. All 1-phase calculations have been explained in detail in [18,4]. The 2-phase solutions are determined by the method of characteristics and numerical evaluation of the 2-phase velocities $v_i^{(2)}$ (11b) using the method presented in Section 3. For these computations, we choose $\rho_0 = 3$ and $L = 1$. Other values give similar results.

The solution of the 2-phase Whitham equations is shown in Fig. 8, where a representative sequence of panels,
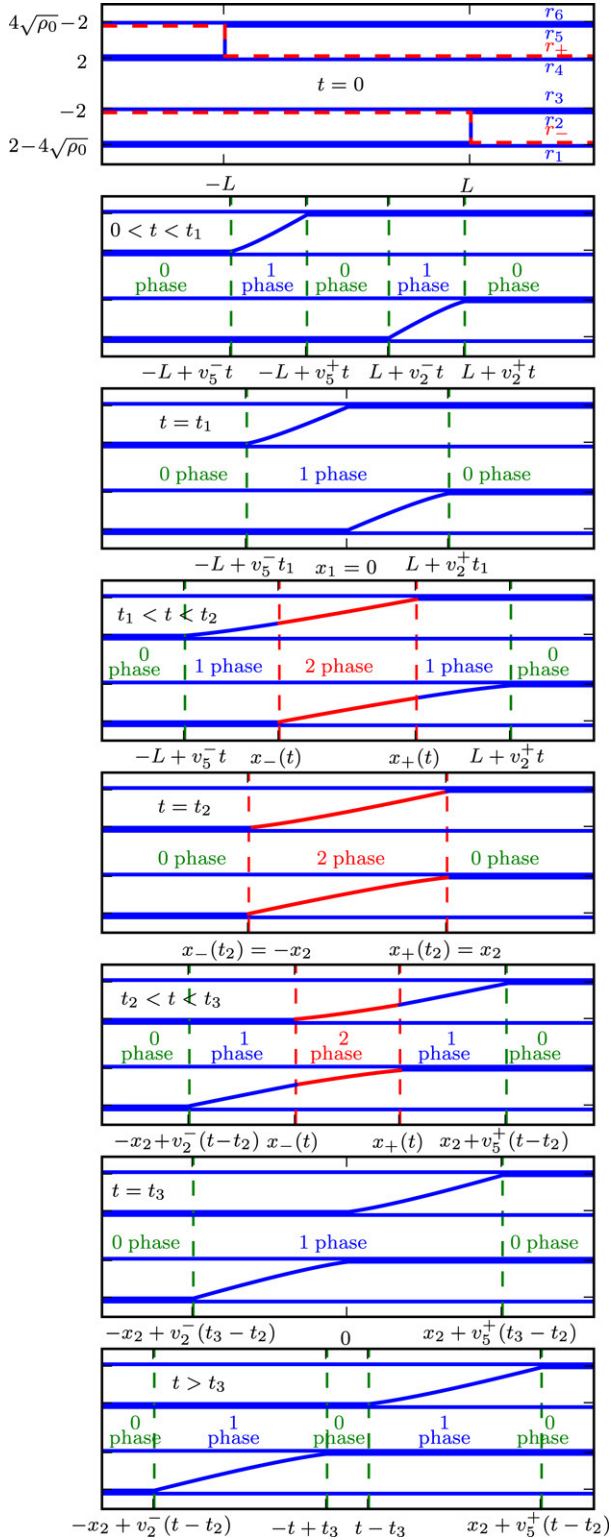
Fig. 8. Evolution of the 2-phase Riemann invariants. The time is shown in the upper left corner for each snapshot.

corresponding to different times in the evolution, is shown. We now describe how this solution was determined.

The only Riemann invariants that vary in space are r_2 and r_5, each having an initial jump. All other Riemann invariants are constant:

$$r_1(x, t) \equiv 2 - 4\sqrt{\rho_0}, \quad r_3(x, t) \equiv -2,$$
$$r_4(x, t) \equiv 2, \quad r_6(x, t) = 4\sqrt{\rho_0} - 2.$$

Whenever we refer to r_1, r_3, r_4, or r_6 in the rest of this section, we assume the constant values given above.

Because the initial data in Fig. 7 satisfy the symmetry condition (15), we know that $r_5(x, t) = -r_2(-x, t)$ for all t and x. Thus, we concentrate on r_2. The solutions we find are of the rarefaction type. A rarefaction wave possesses two constant speeds, one at each edge of the wave. We label the speed corresponding to the left edge of a rarefaction wave in r_i as v_i^-, whereas the right edge speed is labelled v_i^+.

There are three distinct times t_1, t_2, and t_3 (to be defined shortly) that distinguish between different events in the solution process.

Propagation of two isolated DSWs toward each other, $0 < t < t_1 = L(2\sqrt{\rho_0} - 1)/(8\rho_0 - 8\sqrt{\rho_0} + 1)$

In Fig. 7, we see that near $x = L$, $r_5(x, 0) = r_6(x, 0)$, and so there is a degeneracy in the 2-phase representation (e.g., compare with Fig. 3). A 1-phase representation is all that is required to accurately approximate the evolution of the solution. This is to be expected because a single DSW is generated at $x = L$, which propagates until it starts to interact with the DSW originating, by symmetry, at $x = -L$. The rarefaction wave solution for r_2 is self-similar and satisfies

$$\frac{x - L}{t} = v_2^{(1)}(r_1, r_2(x, t), r_3, r_4), \tag{27}$$

when

$$v_2^- < \frac{x - L}{t} < v_2^+.$$

Its associated speeds are

$$v_2^- = \lim_{r_2 \to r_1^+} v_2^{(1)}(r_1, r_2, r_3, r_4) = -\frac{8\rho_0 - 8\sqrt{\rho_0} + 1}{2\sqrt{\rho_0} - 1},$$
$$v_2^+ = \lim_{r_2 \to r_3^-} v_2^{(1)}(r_1, r_2, r_3, r_4) = -\sqrt{\rho_0}. \tag{28}$$

By symmetry, the speeds associated with the rarefaction wave for r_5 are

$$v_5^- = -v_2^+, \quad v_5^+ = -v_2^-. \tag{29}$$

The two rarefaction waves begin to interact at the point (x_1, t_1) where $-L + v_5^+ t_1 = L + v_2^- t_1 = x_1$. We have

$$x_1 = 0, \quad t_1 = -\frac{L}{v_2^-} = \frac{L(2\sqrt{\rho_0} - 1)}{8\rho_0 - 8\sqrt{\rho_0} + 1}.$$

A representative example of the solution for $0 < t < t_1$ and $t = t_1$ is shown in the second and third panels of Fig. 8.

Note that the asymptotic representation of the solution is readily calculated by inserting the values of the locally 1-phase Riemann invariants into the 1-phase solution (5). Comparison of the asymptotic representation and full numerical simulation for a single DSW was performed in [4] and shows excellent agreement.

Initial DSW interaction, $t_1 < t < t_2$

When the two rarefaction waves for r_2 and r_5 begin to overlap, all six Riemann invariants are required to describe the solution; there are no degeneracies. This corresponds to a 2-phase interaction region in the solution, the left and right edges of which we label $x_-(t)$ and $x_+(t)$, respectively. At each edge, one of the Riemann invariants is varying in space and time; therefore, $x_\pm(t)$ are not lines but curves in the xt plane. Because r_2 is constant along the curve $x_-(t)$, this curve is a characteristic associated with r_2 for the solution to the 2-phase Whitham equations. The differential equation describing the left edge is

$$\frac{dx_-}{dt} = \lim_{r_2 \to r_1^+} v_2^{(2)}(r_1, r_2, r_3, r_4, r_5(x_-(t), t), r_6),$$

$$x_-(t_1) = x_1, \tag{30}$$

$$\frac{x_-(t) + L}{t} = v_3^{(1)}(r_3, r_4, r_5(x_-(t), t), r_6).$$

The value of r_5 along this characteristic curve, $r_5(x_-(t), t)$ given implicitly in the last equation above, is known from the rarefaction wave solution created by the initial step at $x = -L$. This implicit equation results from calculating a simple wave solution to the 1-phase Whitham equations

$$\frac{\partial r_5}{\partial t} + v_3^{(1)}(r_3, r_4, r_5, r_6)\frac{\partial r_5}{\partial x} = 0,$$

of the form $r_5(x, t) = r_5(\xi)$, $\xi = (x + L)/t$. Then r_5 satisfies

$$r_5'\left(\xi - v_3^{(1)}(r_3, r_4, r_5(\xi), r_6)\right) = 0,$$

which gives the implicit relation in the last of Eqs. (30). To numerically calculate the limit in (30) due to a degenerate gap, we take $r_2 = r_1 + 2 \cdot 10^{-7}$ when determining the 2-phase velocity. A similar choice is made for all other degenerate gaps numerically evaluated in this work.

The time $t = t_2$ is defined to be the time when the 1-phase regions disappear and the 2-phase region is bordered by 0-phase regions. This occurs when

$$x_-(t_2) = -L + v_5^- t_2 \equiv x_2.$$

By symmetry, $x_+(t) = -x_-(t)$. For later calculations, we will need the value of $r_2(x, t)$ when $x_-(t) < x < x_+(t)$ and $t_1 \leq t \leq t_2$. For this, we use the method of characteristics to solve a Cauchy problem defined below.

By symmetry, $r_2(x, t)$ satisfies the 2-phase equation

$$\frac{\partial r_2}{\partial t} + v_2^{(2)}(r_1, r_2(x, t), r_3, r_4, -r_2(-x, t), r_6)\frac{\partial r_2}{\partial x} = 0. \tag{31}$$

The initial values of r_2 are given on the arc $x_+(t)$, $t_1 \leq t \leq t_2$ in the xt plane implicitly from Eq. (27) with

$$r_{2,0}(s) \equiv r_2(x_+(s), s), \quad t_1 \leq s \leq t_2. \tag{32}$$

Eq. (31) can now be integrated along characteristics as

$$\frac{dr_2}{dt} = 0, \quad \text{along the characteristic curve}$$

$$\frac{dx}{dt} = v_2^{(2)}(r_1, r_2(x, t), r_3, r_4, -r_2(-x, t), r_6).$$

Integrating these equations given the initial data (32) gives the solution implicitly as

$$x = (t - s)v_2^{(2)}(r_1, r_{2,0}(s), r_3, r_4, -r_{2,0}(s), r_6) + x_+(s),$$
$$r_2(x, t) = r_{2,0}(s), \tag{33}$$

where s defines the starting point $(x_+(s), s)$ for the characteristic. This solution is valid only in the range of influence of the initial arc $x_+(t)$, $t_1 \leq t \leq t_2$. An example solution when $t_1 < t < t_2$ and $t = t_2$ is shown in the fourth and fifth panels of Fig. 8.

The representation of the asymptotic solution for the 2-phase interaction region is more complicated than the 1-phase case because it involves evaluating two-dimensional theta functions (as opposed to elliptical functions) with the spatially varying 2-phase Riemann invariants. It is outside the scope of this work to carry at these calculations.

Closing of the DSW interaction region, $t_2 < t < t_3$

At the time $t = t_2$, the 2-phase region of the solution is bordered by 0-phase regions. As soon as $t > t_2$, 1-phase regions appear on either side because of the degeneracies $r_5 = r_4$ and $r_2 = r_3$ on the left and right sides, respectively. The speeds of propagation of the 1-phase fronts into the 0-phase regions are

$$v_2^- = \lim_{r_2 \to r_1^+} v_2^{(1)}(r_1, r_2, r_3, r_6) = -\frac{11\rho_0 - 14\sqrt{\rho_0} + 4}{3\sqrt{\rho_0} - 2},$$
$$v_5^+ = -v_2^-. \tag{34}$$

The evolution of the left boundary between the 1 and 2-phase regions is now described by the following differential equation:

$$\frac{dx_-}{dt} = \lim_{r_5 \to r_4^+} v_5^{(2)}(r_1, r_2(x_-(t), t), r_3, r_4, r_5, r_6),$$
$$x_-(t_2) = x_2, \tag{35}$$

where $r_2(x_-(t), t)$ is determined implicitly by (33) and is within the range of influence of the arc $x_+(t)$, $t_1 \leq t \leq t_2$. Now, the curve $x_-(t)$ is a characteristic associated with r_5 rather than r_2, because r_5 is constant along this curve. Again, $x_+(t) = -x_-(t)$, and so the closing of the DSW 2-phase interaction region occurs when

$$x_-(t_3) = 0.$$

The solution is shown in panels six and seven of Fig. 8.

Propagation of two isolated DSWs away from each other, $t_3 < t$

The 2-phase region closed at $t = t_3$. For times greater than t_3, the solution is described by two 1-phase regions, each representing a DSW, and a 0-phase, constant region in between. This means that a collision of two DSWs results in a 2-phase interaction region that eventually disappears, leaving two DSWs propagating away from each other. The leading edge speeds of each DSW are given in (34), and their trailing edge speeds are

$$v_2^+ = \lim_{r_2 \to r_3^-} v_2^{(1)}(r_1, r_2, r_3, r_6) = -1 = -v_5^-. \tag{36}$$
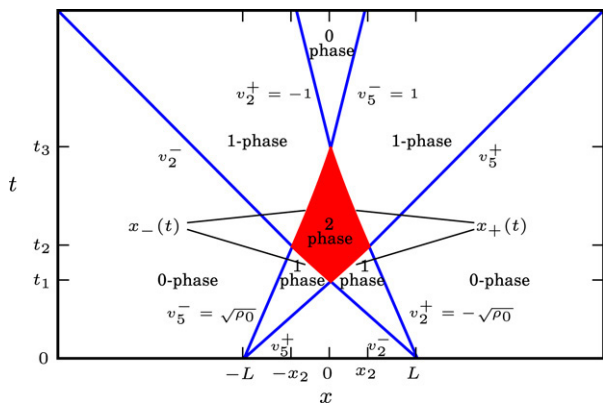
Fig. 9. Bifurcation diagram for a two DSW collision with initial velocity $u_0 = 2\sqrt{\rho_0} - 2$. Different phase regions corresponding to the number of phases in the slowly modulated wave solution are marked. The straight line segments separating 0- and 1-phase regions are calculated from 1-phase DSW theory. Their slopes are the inverses of the front speeds. The filled region bounded by arcs corresponding to boundaries between 1 and 2-phase regions is determined by solving the 2-phase Whitham equations (11).

Note that these speeds are independent of the magnitude of the initial jump in density ρ_0. This result is not limited to our particular choice of the jump in velocity. For any initial velocity $-2\sqrt{\rho_0} + 2 < u_0 \leq 2\sqrt{\rho_0} - 2$, a constant, 0-phase region is formed after the 2-phase interaction occurs. The boundaries of this region move with the speeds ± 1 as in (36), independent of the magnitude of the initial jumps in density ρ_0.

Between these counterpropagating DSWs, the solution is constant because there are two degeneracies, $r_2 = r_3$ and $r_5 = r_4$ (recall Fig. 1). The magnitude of the density and velocity in this region is determined by the degenerate 0-phase Riemann invariants $r_- = r_1$ and $r_+ = r_6$ whereas the rest of the 2-phase Riemann invariants are degenerate:

$$\rho(x, t) = \frac{1}{16}(r_6 - r_1)^2 = \left(2\sqrt{\rho_0} - 1\right)^2,$$

$$u(x, t) = \frac{1}{2}(r_6 + r_1) = 0, \quad |x| < t - t_3, \quad t_3 < t.$$

The solution is shown in the last panel of Fig. 8.

We have detailed the collision process for two pure DSWs by solving the 2-phase Whitham modulation equations. The results show that two DSWs propagating toward one another interact, giving rise to a 2-phase region. This region eventually closes, and two counterpropagating DSWs of larger trailing edge density amplitude but smaller trailing edge speed emerge, leaving a constant region in their wake. This interaction process is represented in the bifurcation diagram of Fig. 9. The line segments represent boundaries between 0 and 1-phase regions, the slopes of which are the inverse of the speeds given in Eqs. (28), (29), (34) and (36). The filled region bounded by arcs is the 2-phase interaction region as calculated by Eqs. (30) and (35). All boundaries between different phase regions are characteristics associated with the 1 or 2-phase equations.

5.1.3. Comparison with full numerical simulation: $u_0 = 2\sqrt{\rho_0} - 2$

In order to verify the validity of the Whitham averaging procedure, we performed full numerical simulations of the NLS

equation (1) with a slightly smoothed version of the initial data (25) using a split-step Fourier numerical method [30]. This method assumes a periodic solution (i.e. periodic boundary conditions are applied), so we localize the initial data in space and verify that the smooth transitions to zero density do not affect the shock solution. It is important to note that the initial data was assumed discontinuous for the Whitham averaging analysis. Even though the numerical simulations were performed with smoothed versions of the initial discontinuities, very good agreement with the asymptotic Whitham theory is found. This demonstrates the robustness of the Whitham approach.

All the calculations in this work were performed with $\varepsilon = 0.02$ in Eq. (1) except where noted. The results for the density evolution are shown in Fig. 10 and for the velocity evolution in Fig. 11. The eight evolution times pictured correspond to the eight evolution times used in Fig. 8, the solution of the Whitham equations. The boundaries between the different phase regions and the predicted times t_1, t_2, and t_3 are in excellent agreement with the numerical solutions.

Another view of the solution is shown in Fig. 12, a contour plot in the xt plane of the numerical solution for the density ρ with the bifurcation diagram in Fig. 9 overlaid on top of it. The theoretically determined boundaries between the different phase regions agree well with the full numerical simulation. The 2-phase region is characterized by interacting nonlinear waves that form a hexagonal lattice pattern [18]. Fig. 13 shows a close-up of this pattern. A linear superposition of waves predicts a diamond lattice pattern. However, the nonlinearity induces a phase shift in these interacting waves near the 1-phase boundaries (the soliton limit) hence a hexagonal pattern remains. The 1-phase regions correspond to noninteracting propagating modulated waves.

5.1.4. Initial data regularization: $u_0 = 0$

The specific choice $u_0 = 2\sqrt{\rho_0} - 2$ in (25) gave two pure DSWs propagating toward one another. We now show that for $u_0 = 0$, the situation is almost the same except two rarefaction waves are generated that have a small influence on the solution. Similar qualitative behaviour is observed for any choice of u_0 in the range $|u_0| < 2\sqrt{\rho_0} - 2$, corresponding to case III in Fig. 5.

The case $u_0 = 0$ is of physical interest in Bose–Einstein condensates, where an initial, broad dip in a quasi-1D condensate is formed with a repulsive laser while the dilute gas of bosons is cooled into the condensed state. There is no initial phase gradient in the condensate wavefunction, so $u_0 = 0$. This procedure produces a dip in the density represented approximately by the initial data in the top of Fig. 4.

The initial data regularization is depicted in Fig. 14 (see Section 4 for a discussion of this regularization method). The difference from the previous case shown in Fig. 7 is that the four Riemann invariants r_2, r_3, r_4, and r_5 exhibit jumps initially, as opposed to jumps in r_2 and r_5 previously. The proof that a global solution exists for these initial data given in Section 4 still holds in this case because each Riemann invariant's evolution will be coupled to at most one other Riemann invariant. At any given time and space,
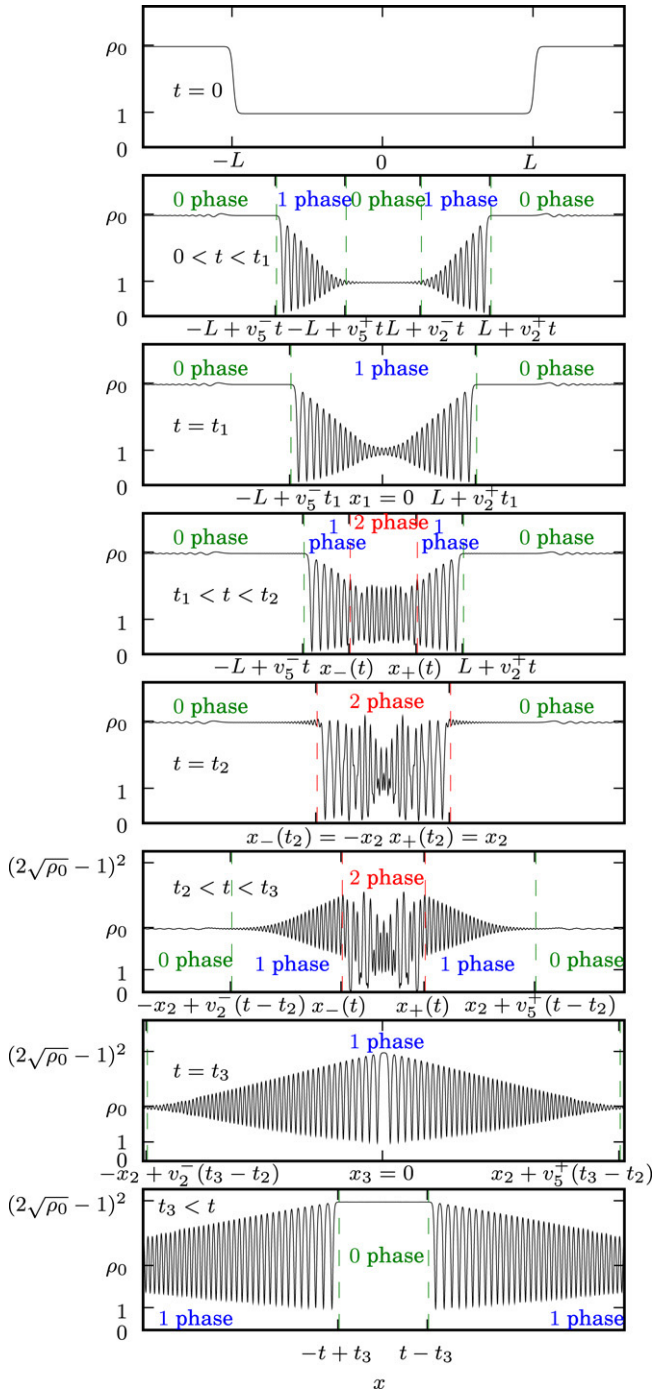
Fig. 10. Numerical solution of the density ρ for the collision of two DSWs. Dashed, vertical lines correspond to theoretically determined boundaries between different phase regions (see Figs. 8 and 9). Note the 2-phase interaction region that develops and changes into a 0-phase constant region with two DSWs propagating away from each other. Parameters are $\rho_0 = 3$ and $L = 1$.

Fig. 11. Numerical solution of the velocity u for the collision of two DSWs with the theoretically determined boundaries between different phase regions marked with vertical dashed lines. Parameters are $\rho_0 = 3$ and $L = 1$.

at most two Riemann invariants will be locally nonconstant, hence are described by a system of at most two hyperbolic equations. Note that the separability condition in Eq. (20) is not satisfied for this regularization. As was mentioned earlier the separability condition is sufficient but not necessary for the dispersive regularization. For this regularization, the Riemann invariants do not cross hence one has a global solution.

5.1.5. Solution of the Whitham equations: $u_0 = 0$

We have computed the solution of the Whitham equations with the initial data shown in Fig. 14 for the choices $\rho_0 = 3$ and $L = 1$. These calculations give the boundaries between different phase regions, which are shown in the bifurcation diagram of Fig. 15. The dashed rays correspond to the edges of the 0-phase rarefaction waves generated at each initial step. All the speeds are marked in the diagram and are computed, as in Section 5.1.2, by taking appropriate limiting values of the
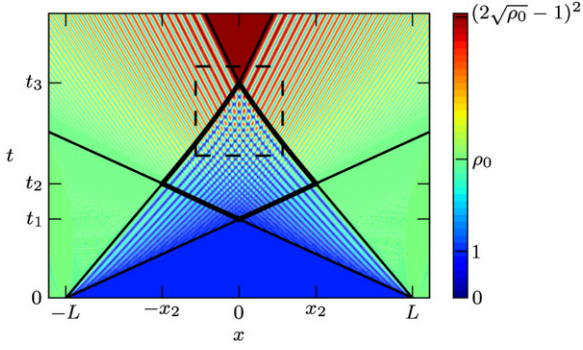
Fig. 12. Contour plot of numerical solution with overlay of bifurcation diagram showing the accuracy of Whitham theory. See Fig. 13 for a close-up of the 2-phase interaction region inside the dashed box.
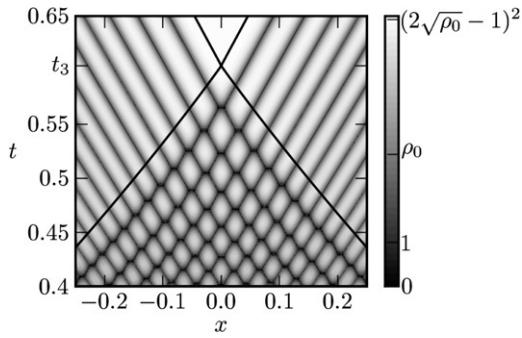
Fig. 13. Close-up of 2-phase interaction region from Fig. 12. The 2-phase region near the 1-phase boundaries (the soliton limit) is characterized by a hexagonal lattice pattern corresponding to interacting nonlinear waves.
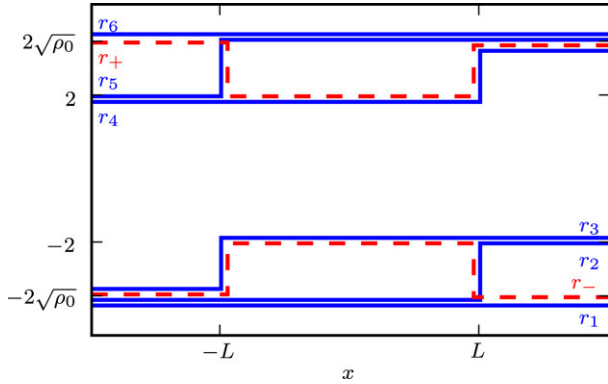
Fig. 14. Initial data regularization for a two DSW collision process with zero initial velocity.

Whitham velocities $v_i^{(1)}$ or 0-phase velocities $v_\pm$. Their values are

$$v_3^- = v_-\left(-2\sqrt{\rho_0}, 2\sqrt{\rho_0}\right) = -\sqrt{\rho_0} = -v_4^+,$$

$$v_3^+ = v_-\left(-2, 2\sqrt{\rho_0}\right) = \frac{1}{2}\sqrt{\rho_0} - \frac{3}{2} = -v_4^-,$$

$$v_{2i}^- = \lim_{r_2 \to -2\sqrt{\rho_0}^+} v_2^{(1)}\left(-2\sqrt{\rho_0}, r_2, -2, 2\right) = \frac{1 - 2\rho_0}{\sqrt{\rho_0}} = -v_{5i}^+$$

$$v_{2i}^+ = \lim_{r_2 \to -2^-} v_2^{(1)}\left(-2\sqrt{\rho_0}, r_2, -2, 2\right)$$
$$= -\frac{1}{2}\left(\sqrt{\rho_0} + 1\right) = -v_{5i}^-,$$
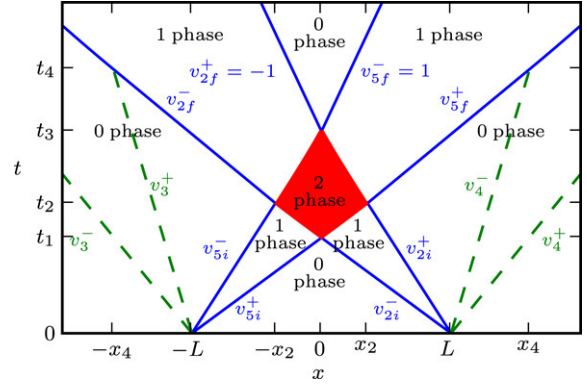
Fig. 15. Phase regions for a two DSW collision process with zero initial velocity, similar to the pure shock case depicted in Fig. 9. The dashed rays represent the boundaries of two 0-phase rarefaction waves.

$$v_{2f}^+ = \lim_{r_2 \to -2\sqrt{\rho_0}^+} v_2^{(1)}\left(-2\sqrt{\rho_0}, r_2, -2, 2\sqrt{\rho_0}\right)$$
$$= -1 = -v_{5f}^-,$$

$$v_{2f}^- = \lim_{r_2 \to -2^-} v_2^{(1)}\left(-2\sqrt{\rho_0}, r_2, -2, 2\sqrt{\rho_0}\right)$$
$$= -\frac{11\rho_0 - 6\sqrt{\rho_0} - 1}{6\sqrt{\rho_0} - 2} = -v_{5f}^+.$$

The symmetry in the results comes from the symmetry condition (15) satisfied by the initial data.

As before, a 0-phase region is created after the interaction process. The speed of the right (left) boundary of this region with the 1-phase region is $v_{2f}^+ = 1$ ($v_{5f}^- = -1$), independent of the initial data chosen. As mentioned previously, this is a general result that holds for $-2\sqrt{\rho_0} + 2 < u_0 \le 2\sqrt{\rho_0} - 2$.

5.1.6. Comparison with full numerical simulation: $u_0 = 0$

The numerical solution for the density ρ is shown in Fig. 16, where we have assumed that $\varepsilon = 0.02$. There is excellent agreement between the simulation and Whitham theory shown by the theoretically determined boundaries (dashed vertical lines) and the numerical solution. A view of the solution as a contour plot in the xt plane is shown in Fig. 17 overlayed with the bifurcation diagram from Fig. 15. A hexagonal lattice pattern corresponding to nonlinear wave interactions is visible in the 2-phase region, whereas the 1-phase regions are characterized by undisturbed waves. The 0-phase regions are constant or involve rarefaction waves with small amplitude oscillations that disappear in the limit $\varepsilon \to 0$.

5.1.7. Complete classification for arbitrary initial velocity u_0

Arbitrary choices for the initial steps in velocity u_0 give qualitatively different behaviour. We will not present the full analysis here; we will state only the main results. The regions below refer to those shown in Fig. 5.

Region I, $u_0 > 2\sqrt{\rho_0} + 2$

For region I, corresponding to a large initial velocity, the 2-phase interaction region remains for all time. It does not develop into a constant, 0-phase region. The bifurcation diagram for the specific choice $\rho_0 = 3$ and $u_0 = 2\sqrt{\rho_0} + 4$ is shown in Fig. 18. Because of the initial generation of four
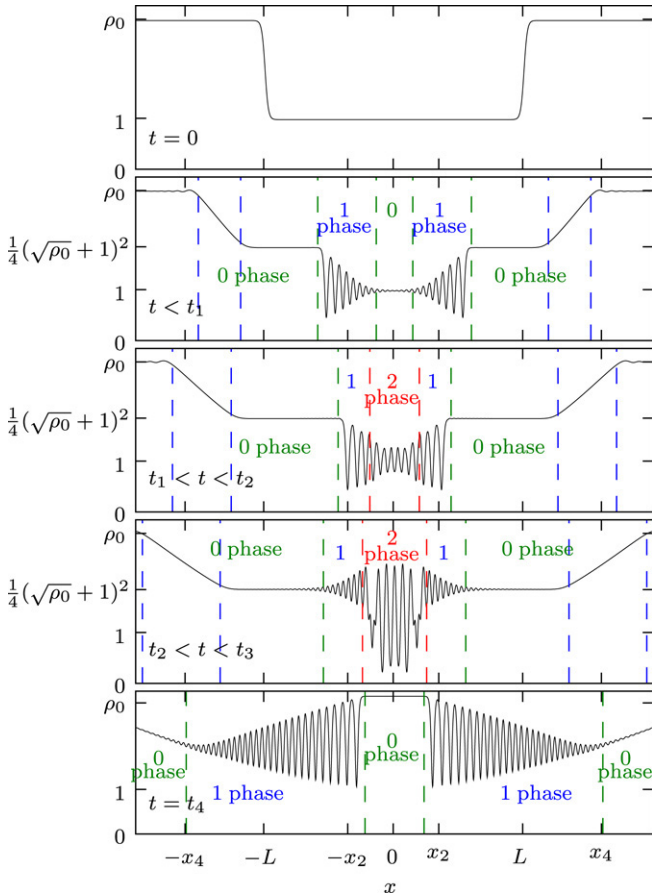
Fig. 16. Evolution of the density ρ from numerical simulation of equations (2) for the case $u_0 = 0$ in (25). Note the generation of two rarefaction waves. Parameters are $\rho_0 = 3$ and $L = 1$.
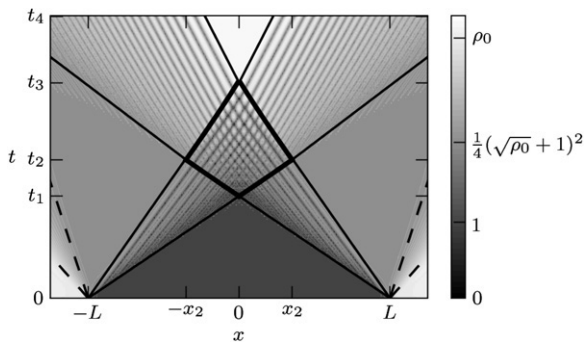
Fig. 17. Contour plot of numerical solution for a DSW collision with the bifurcation diagram in Fig. 15 overlaid on top. The 2-phase region is characterized by a hexagonal lattice pattern corresponding to nonlinear interacting waves [18].

DSWs (see Fig. 6), the interaction process is more complicated than in the previous cases considered. The numerical solution to Eq. (1) with $\varepsilon = 0.15$ is shown in Fig. 19. The generation of four DSWs and their 2-phase interaction is apparent.

Although the 2-phase interaction region expands in time, it nevertheless becomes degenerate as $t \to \infty$. This can be understood by considering the solution to the 2-phase Whitham equations shown in Fig. 20. As time increases, the Riemann invariants r_3 and r_4 move closer to each other. This corresponds
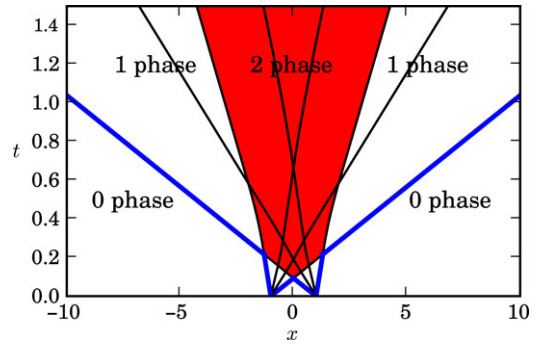
Fig. 18. An example bifurcation diagram in the characteristic xt plane for a collision process with large initial velocity $u_0 > 2\sqrt{\rho_0}$ corresponding to regions I and II in Fig. 5. The 2-phase interaction region (filled) expands in time, different from the previous cases analysed. The curves represent edges of the calculated rarefaction wave solutions for the 2-phase Riemann invariants (see Fig. 20 for the solution at $t = 1.5$). The parameters are $L = 1$, $\rho_0 = 3$, and $u_0 = 2\sqrt{\rho_0} + 4$.
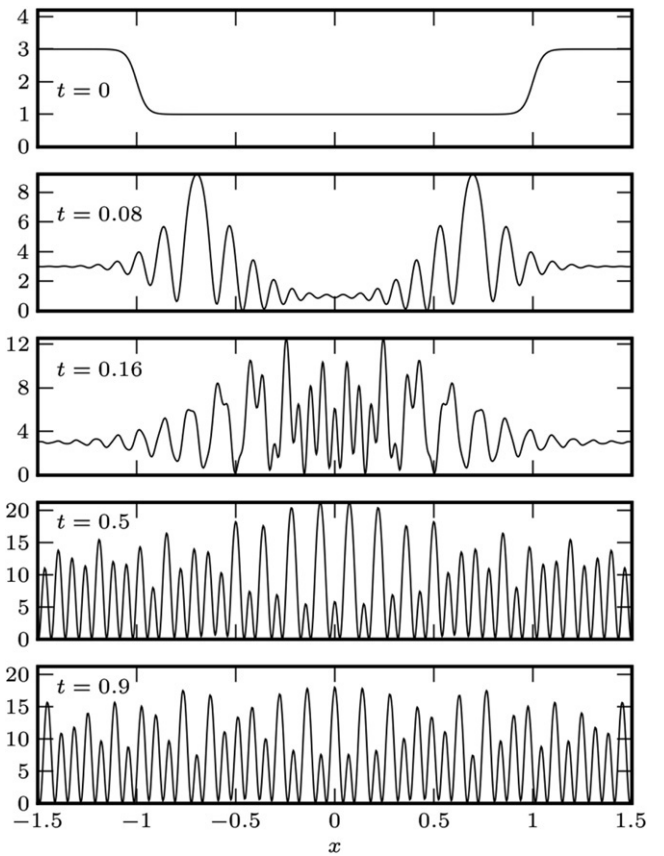
Fig. 19. Density ρ of the numerical solution to the NLS equation (1) with two step initial data (25) for large initial velocity $u_0 = 2\sqrt{\rho_0} + 4$ at different times (noted on left of each plot). In this regime, the 2-phase interaction region remains for all time but is asymptotically degenerate. The parameters are $L = 1$, $\varepsilon = 0.15$, and $\rho_0 = 3$.

to the closure of one of the gaps in the spectrum of (10), and thus a degeneracy. As this gap closes, the modulated 2-phase solution of the NLS equation becomes closer to a modulated 1-phase solution. For example, it could be a soliton propagating on a single phase periodic background. This behaviour can be understood as the nonlinear superposition of two solutions, a
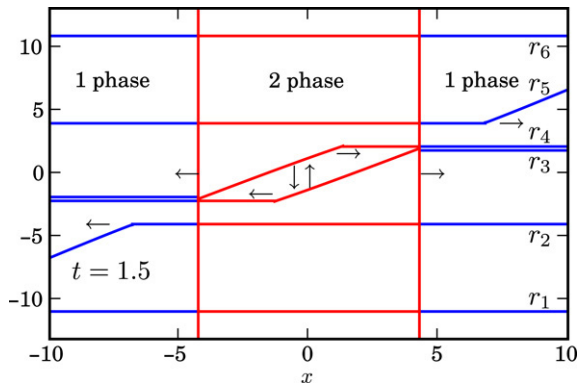
Fig. 20. Calculated solution of the 2-phase Whitham equations via characteristics for a DSW collision with large initial velocity. As time increases, the Riemann invariants r_3 and r_4 get closer to one another. This corresponds to the closure of one of the gaps in the spectrum of (10), and thus a degeneracy.

1-phase (periodic) solution and a soliton, as was discussed in the context of the KdV equation [31,32].

Between the counterpropagating DSWs and the 2-phase region are two nonmodulated periodic waves. This is different from what occurs when the initial velocity is in region II of Fig. 5 where the counterpropagating DSWs are connected *directly* to the 2-phase region.

In Ref. [33] Grava and Tian proved that, for appropriate initial data giving rise to modulated 2-phase behaviour, the long-time state of the KdV equation is described by a modulated 1-phase or 0-phase solution. In contrast, for the defocusing NLS equation we have demonstrated numerically the existence of modulated 2-phase states for long times, although they become increasingly degenerate as time increases.

Region II, $2\sqrt{\rho_0} < u_0 < 2\sqrt{\rho_0} + 2$

The long time state for region II in Fig. 5 is the same as for region I with the exception that the two DSWs are connected directly to the 2-phase region without the nonmodulated periodic waves in between (not shown here).

Region III, $2\sqrt{\rho_0} - 2 < u_0 < 2\sqrt{\rho_0}$

The long-time behaviour of the asymptotic solution for region III (see Fig. 5) is similar to what we have already presented in detail for $u_0 = 2\sqrt{\rho_0} - 2$ and $u_0 = 0$. Initially, two DSWs are generated at each initial step (see Fig. 6). The two central DSWs propagate toward one another, generate a 2-phase interaction region, and then a constant, 0-phase region emerges after the interaction process. The two DSWs that emerge from the interaction region eventually interact with the remaining two DSWs via a 2-phase merging interaction that form as fast DSWs overtake slower ones. We will discuss the merging interaction in Section 5.2. For large enough time, the solution consists of two counterpropagating DSWs connected by a constant, 0-phase region.

Region IV, $-2\sqrt{\rho_0} + 2 < u_0 < 2\sqrt{\rho_0} - 2$

We have analysed the behaviour in region IV extensively with the specific choices $u_0 = 2\sqrt{\rho_0} - 2$ and $u_0 = 0$. All other collisions with u_0 in region IV behave qualitatively the same. A DSW and rarefaction wave are generated at each initial step

(see Fig. 6). The central, counterpropagating DSWs interact via a modulated 2-phase region. Two counterpropagating DSWs emerge from the interaction region leaving behind a constant, 0-phase region. This central region of constant density and velocity has right/left boundaries propagating with the speeds ± 1, independent of the initial jump in density ρ_0 and velocity u_0. The DSWs eventually overtake the counterpropagating rarefaction waves that were generated at the initial steps. Thus two DSWs remain.

Region V, $u_0 < -2\sqrt{\rho_0} + 2$

Region V leads to the generation and interaction of rarefaction waves, hence is completely explained within the framework of a 0-phase description. No shock phenomena are observable in this region so we do not analyse it any further.

5.2. Merging

Another type of shock interaction occurs when a faster shock overtakes a slower one. For this, we consider two initial steps, one on top of the other (see also Fig. 21)

$$\rho(x, 0) = \begin{cases} \rho_1 & x < -L \\ \rho_0 & |x| < L \\ 1 & L < x \end{cases}, \quad \rho_1 > \rho_0 > 1,$$

$$u(x, 0) = \begin{cases} u_1 & x < -L \\ u_0 & |x| < L \\ 0 & L < x. \end{cases} \tag{37}$$

This initial data can be generalized with the rescaling in Eqs. (26). The initial data (37) then becomes

$$\tilde{\rho}(\tilde{x}, 0) = \begin{cases} \rho_u & \tilde{x} < -\tilde{L} \\ \rho_l & |\tilde{x}| < \tilde{L} \\ \rho_m & \tilde{L} < \tilde{x} \end{cases}, \quad \rho_u > \rho_l > \rho_m,$$

$$\tilde{u}(\tilde{x}, 0) = \begin{cases} u_u & \tilde{x} < -\tilde{L} \\ u_l & |\tilde{x}| < \tilde{L} \\ u_m & \tilde{L} < \tilde{x}, \end{cases}$$

where $\rho_u = \rho_1 \rho_m$, $\rho_l = \rho_0 \rho_m$, $u_u = \sqrt{\rho_m} u_1 + u_m$, $u_l = \sqrt{\rho_m} u_0 + u_m$, and $\tilde{L} = L/\sqrt{\rho_m}$. To simplify the analysis, we assume pure shock initial conditions so that

$$u_1 = 2\sqrt{\rho_1} - 2, \quad u_0 = 2\sqrt{\rho_0} - 2. \tag{38}$$

A complete classification of the two step initial value problem will be undertaken in a future work.

5.2.1. Initial data regularization

Fig. 22 depicts a choice of initial data for the 2-phase Riemann invariants that satisfies the regularization conditions (20) for the initial value problem (37) (see Section 4 for a discussion of how and why this regularization is valid). We now seek the solution of the 0, 1, or 2-phase Whitham equations (4), (7), or (11), as appropriate, subject to the initial data in Fig. 22.
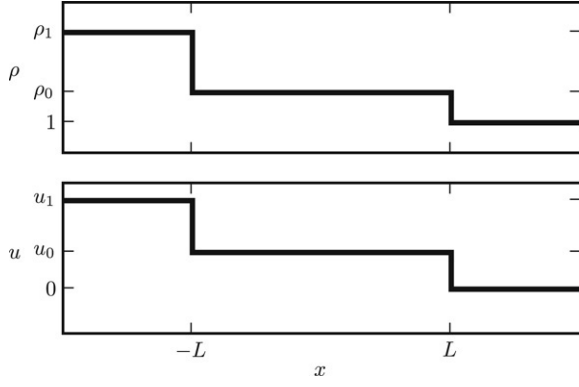
Fig. 21. Initial data for the case of a merger of two DSWs.
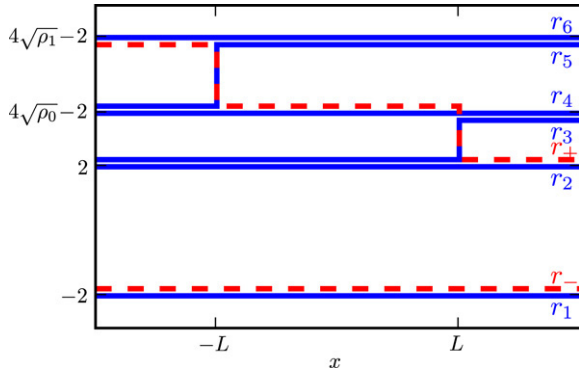
Fig. 22. Initial data regularization for the case of a merger of two DSWs.

5.2.2. Solution of the Whitham equations

In this section we outline the solution of the Whitham equations via the method of self-similar solutions and characteristics. In contrast to the collision case, the initial data in Fig. 22 does not maintain the symmetry (15). Therefore, we use a more general numerical scheme to integrate the 2-phase Whitham equations along characteristics. As in the collision case, the solution method is different, depending on the evolution time. The only two Riemann invariants that have nontrivial spatial and temporal dependences are r_3 and r_5 while the others are constant

$$r_1(x, t) \equiv -2, \quad r_2(x, t) \equiv 2,$$
$$r_4(x, t) \equiv 4\sqrt{\rho_0} - 2, \quad r_6(x, t) \equiv 4\sqrt{\rho_1} - 2.$$

Whenever we refer to $r_1, r_2, r_4,$ or r_6 in the rest of this section, we assume the constant values given above.

The main features of the solution, such as phase boundaries outlined below, are shown in the bifurcation diagram of Fig. 23.

Propagation of 2 isolated DSWs, $0 < t < t_1$

Near $x = -L$, $r_2(x, 0)$ and $r_3(x, 0)$ are degenerate, so the evolution of r_5 is described by the 1-phase equation,

$$\frac{\partial r_5}{\partial t} + v_3^{(1)}(r_1, r_4, r_5, r_6)\frac{\partial r_5}{\partial x} = 0.$$

We solve for the self-similar rarefaction wave satisfying the implicit relation

$$\frac{x + L}{t} = v_3^{(1)}(r_1, r_4, r_5(x, t), r_6), \tag{39}$$
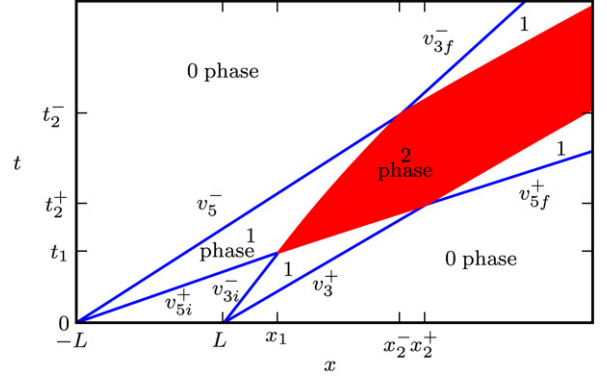
Fig. 23. Bifurcation diagram for DSW merging in the characteristic xt plane. The number of phases required to describe the asymptotic solution is shown along with the speeds associated with different 1-phase fronts. The 2-phase interaction region (filled) eventually closes as shown in Figs. 25 and 26.

in the region

$$v_5^- < \frac{x + L}{t} < v_{5i}^+, \quad 0 < t < t_1,$$
$$v_5^- = \lim_{r_5 \to r_4^+} v_3^{(1)}(r_1, r_4, r_5, r_6)$$
$$= \sqrt{\rho_1} + 2\sqrt{\rho_0} - 2,$$
$$v_{5i}^+ = \lim_{r_5 \to r_6^-} v_3^{(1)}(r_1, r_4, r_5, r_6)$$
$$= \frac{8\rho_1 - (4\sqrt{\rho_0} + 4)\sqrt{\rho_1} - \rho_0 + 2\sqrt{\rho_0}}{2\sqrt{\rho_1} - \sqrt{\rho_0}}.$$

A similar solution is found for r_3 centred at $x = L$:

$$\frac{x - L}{t} = v_3^{(1)}(r_1, r_2, r_3(x, t), r_4), \tag{40}$$

defined in the region

$$v_{3i}^- < \frac{x - L}{t} < v_3^+, \quad 0 < t < t_1,$$
$$v_{3i}^- = \lim_{r_3 \to r_2^+} v_3^{(1)}(r_1, r_2, r_3, r_4)$$
$$= \sqrt{\rho_0}$$
$$v_3^+ = \lim_{r_3 \to r_4^-} v_3^{(1)}(r_1, r_2, r_3, r_4)$$
$$= \frac{8\rho_0 - 8\sqrt{\rho_0} + 1}{2\sqrt{\rho_0} - 1}.$$

These two rarefaction solutions correspond to two copropagating DSWs. The location and time of interaction of these two waves (x_1, t_1) are given by

$$-L + v_{5i}^+ t_1 = L + v_{3i}^- t_1 \equiv x_1, \quad t_1 = \frac{2L}{v_{5i}^+ - v_{3i}^-}.$$

Note that due to the ordering property (24), $v_{5i}^+ > v_{3i}^-$.

Initial DSW interaction, $t_1 < t < t_2^+$

Now that the two Riemann invariants r_3 and r_5 have a region in common where they both are nonconstant, their evolution is described locally by the 2-phase Whitham equations (11). The boundaries of this interaction region are characteristics that

we label $x_-(t)$ and $x_+(t)$ for the left and right boundaries, respectively. The left boundary is a characteristic along which r_3 is constant and satisfies

$$\frac{dx_-}{dt} = \lim_{r_3 \to r_2^+} v_3^{(2)}(r_1, r_2, r_3, r_4, r_5(x_-(t), t), r_6),$$ (41)

$$x_-(t_1) = x_1,$$

where $r_5(x_-(t), t)$ is determined by Eq. (39). The right boundary is a characteristic associated with constant r_5 and satisfies

$$\frac{dx_+}{dt} = \lim_{r_5 \to r_6^-} v_5^{(2)}(r_1, r_2, r_3(x_+(t), t), r_4, r_5, r_6),$$ (42)

$$x_+(t_1) = x_1,$$

with $r_3(x_+(t), t)$ determined by Eq. (40). The right boundary, $x_+(t)$, of the 2-phase interaction region satisfies (42) until the time when it intersects the right edge of the rarefaction wave solution for r_3,

$$x_+(t_2^+) = L + v_3^+ t_2^+ \equiv x_2^+.$$

Emergence of 1-phase front, $t_2^+ < t < t_2^-$

After the time t_2^+, a 1-phase front emerges from the right edge of the 2-phase interaction region due to the degeneracy $r_3 = r_4$ (see Fig. 1). The speed of this front is

$$v_{5f}^+ = \lim_{r_5 \to r_6^-} v_3^{(1)}(r_1, r_2, r_5, r_6)$$

$$= \frac{8\rho_1 - 8\sqrt{\rho_1} + 1}{2\sqrt{\rho_1} + 1}.$$

This speed corresponds exactly to the front speed of a single, pure DSW connecting the density ρ_1 to the background density 1 [4].

The left boundary of the 2-phase region, $x_-(t)$, satisfies Eq. (41) until the time t_2^-, when it intersects the left edge of the rarefaction wave solution for r_5,

$$x_-(t_2^-) = -L + v_5^- t_2^- \equiv x_2^-.$$

Emergence of 1-phase trailing edge, merged DSWs, $t_2^- < t$

For times greater than t_2^-, the trailing edge of a DSW 1-phase region emerges from the 2-phase interaction region. The speed of this trailing edge is

$$v_{3f}^- = \lim_{r_3 \to r_2^+} v_3^{(1)}(r_1, r_2, r_3, r_6)$$

$$= \sqrt{\rho_1},$$

corresponding to the trailing edge speed of a single, pure DSW with a jump in density of ρ_1 from a normalized background density of 1 [4]. The trailing and leading edges of a pure DSW have emerged from the 2-phase interaction region representing the merger of the two initial DSWs. We now determine the boundaries of the interaction region.
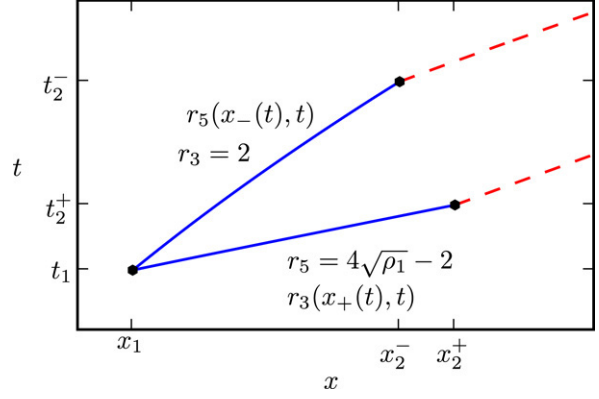
Fig. 24. Cauchy initial data for calculation of the 2-phase interaction region in the merging problem. The solid arcs correspond to those given in Eq. (43), the initial curve on which r_3 and r_5 are given. The dashed arcs correspond to the calculated characteristics emanating from the points (x_2^-, t_2^-) and (x_2^+, t_2^+) that bound the region of influence of the initial data.

We have a Cauchy problem for r_3 and r_5 with initial data given on the initial 2-phase boundaries. Specifically, we solve

$$\frac{\partial r_3}{\partial t} + v_3^{(2)}(r_1, r_2, r_3(x, t), r_4, r_5(x, t), r_6)\frac{\partial r_3}{\partial x} = 0$$

$$\frac{\partial r_5}{\partial t} + v_5^{(2)}(r_1, r_2, r_3(x, t), r_4, r_5(x, t), r_6)\frac{\partial r_5}{\partial x} = 0,$$

subject to the initial data

$$r_{3,0}(s) \equiv r_3(x(s), s), \quad r_{5,0}(s) \equiv r_5(x(s), s),$$

$$(x(s), s) \in \{(x_-(t), t) \mid t_1 \leq t \leq t_2^-\}$$ (43)

$$\cup \{(x_+(t), t) \mid t_1 \leq t \leq t_2^+\}.$$

The values $r_3(x(s), s)$ and $r_5(x(s), s)$ were calculated while solving Eqs. (42) and (41) respectively. The initial data for this Cauchy problem is shown in Fig. 24.

We solve this Cauchy problem numerically along characteristics with a method presented in chapter 7.3 of [34]. This method involves calculating the characteristics of constant r_3 and r_5 in the xt plane with a first order discretization scheme. The intersections of these characteristics defines an irregular grid in the region of influence of the initial arc (43) where the solution is known.

The boundaries between the 2-phase interaction region and the emerging 1-phase regions are characteristics emanating from the endpoints of the initial arc (43). The left boundary $x_-(t)$ is the characteristic emanating from the point (x_2^-, t_2^-) with r_5 constant, while the right boundary $x_+(t)$ is the characteristic emanating from the point (x_2^+, t_2^+) with r_3 constant. These two characteristics propagate toward each other, as shown in Figs. 25 and 26, corresponding to the gradual closure of the 2-phase region. We find numerically that the 2-phase region closes in finite time. The solution of the 2-phase Whitham equations we have found is independent of ε and therefore this result, the closure of the 2-phase region, holds asymptotically for the zero dispersion limit of the NLS equation (1). Note that the 2-phase region closes at a cusp with zero angle because the slopes of the rightmost front $x_+(t)$ and the leftmost front $x_-(t)$ are the same at the closing point (x_3, t_3).
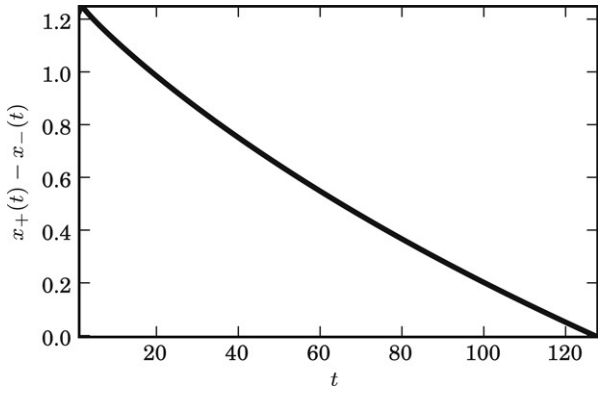
Fig. 25. Width of the 2-phase interaction region as a function of time, showing that its closure occurs in finite time. The initial data satisfies $\rho_0 = 2$, $\rho_1 = 4$, and $L = 0.5$.
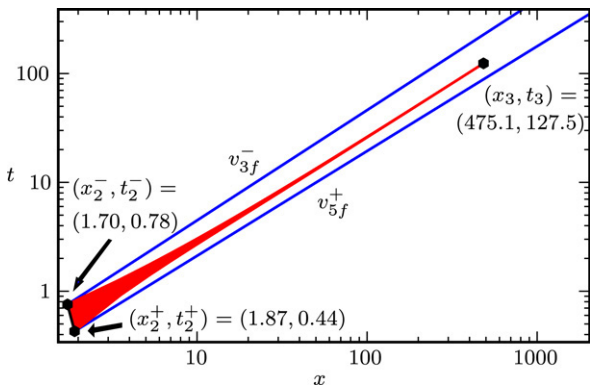
Fig. 26. Log–log plot of the characteristic xt plane, showing the closure of the 2-phase interaction region at the point (x_3, t_3). The boundary of the 2-phase region closes off in a cusp because $dx_-/dt = dx_+/dt$ at the closure point. The parameters are $\rho_0 = 2$, $\rho_1 = 4$, and $L = 0.5$.

The analysis we have presented for this interaction process shows that when a faster DSW overtakes a slower one, the two interact but eventually merge into a single DSW. This behaviour is valid for any choice $\rho_1 > \rho_0 > 1$ as long as the initial velocities satisfy Eqs. (38).

5.2.3. Comparison with full numerical simulations

We solve Eq. (1) numerically with the choice $\varepsilon = 0.02$. Fig. 27 depicts the evolution of the density ρ from the initial data (37). The analytically determined boundaries between 0, 1, and 2-phase regions are marked with vertical dashed lines. The agreement between the asymptotic Whitham averaging theory and numerical solution of the full equations is excellent. This figure depicts the initial generation of two DSWs, their interaction, and the emergence of trailing and leading 1-phase regions representing the merger of the original two DSWs.

A further comparison is shown in Fig. 28, where a contour plot of the numerical solution is shown overlayed with the bifurcation diagram of Fig. 23 (see the hexagonal lattice in the zoomed in contour plot of Fig. 29).

Note that the width of the interaction region is decreasing as a function of time, in agreement with the asymptotic results, but it would be extremely difficult to observe the closure of this
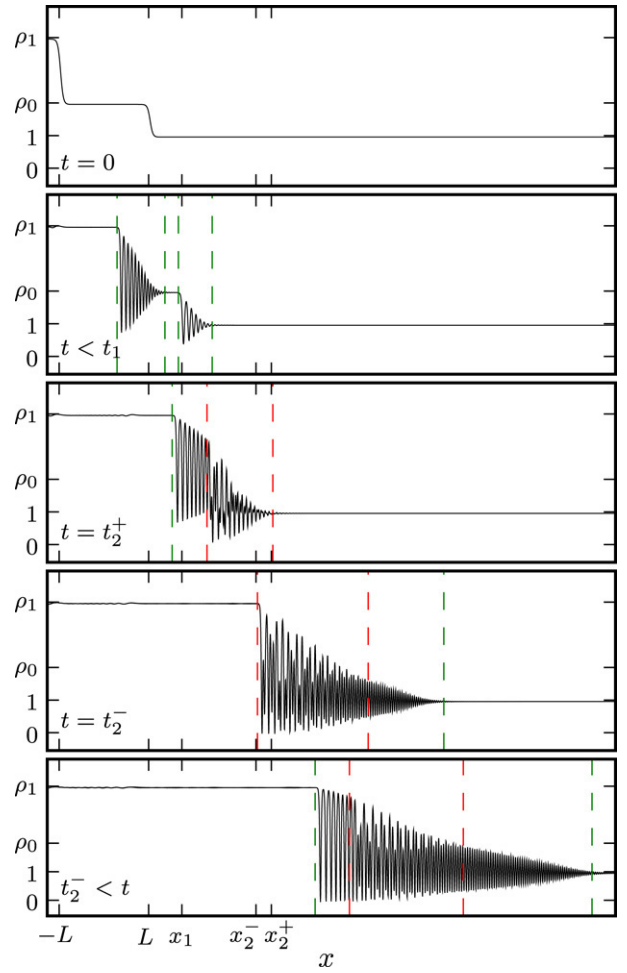
Fig. 27. Evolution of the density for a DSW merging interaction as determined from numerical simulation. The vertical dashed lines correspond to boundaries between different phase regions as determined from Whitham theory (see Fig. 23). The parameters are $\rho_0 = 2$, $\rho_1 = 4$, and $L = 0.5$.
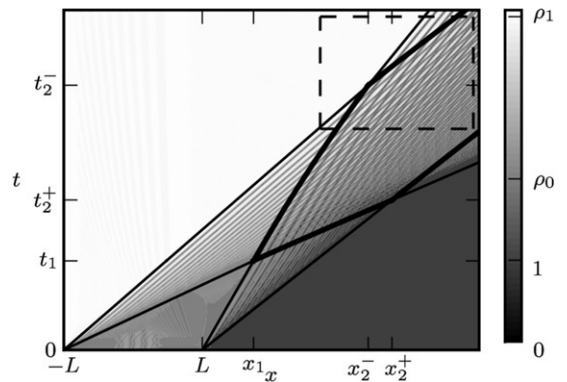
Fig. 28. Contour plot of numerical solution for a DSW merging interaction in the xt plane overlayed with the bifurcation diagram from Fig. 23. The 1-phase regions are characterized by propagating waves whereas the 2-phase region depicts two wave interactions as a lattice. See Fig. 29 for a closer look at the dashed rectangular region.

interaction region numerically. Whitham averaging performed in Section 5.2.2 provides a means to observe this closure.
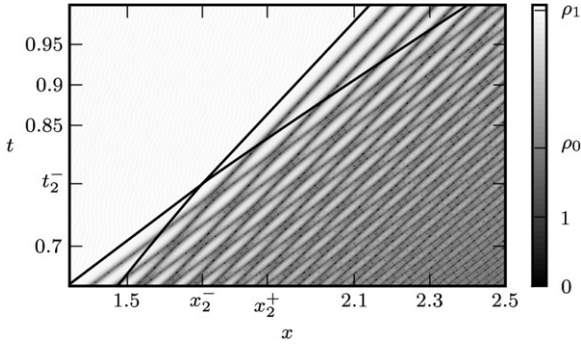
Fig. 29. Zoomed in region of the contour plot of Fig. 28 (see dashed box). Note the lattice pattern.

6. Classical shock interaction

For certain initial data, the long-term, qualitative behaviour of DSW interaction is similar to the classical interaction of VSWs. We now explain why this is the case. See, for example [10], for a detailed analysis of VSW interaction theory.

6.1. Classical collision

Consider the dissipative regularization of the Euler equations

$$\rho_t + (\rho u)_x = 0$$
$$(\rho u)_t + \left(\rho u^2 + \frac{1}{2}\rho^2 \right)_x = 0, \tag{44}$$

with the initial conditions (25) for the special case of two pure VSWs, $u_0 = (\rho_0 - 1)\sqrt{\frac{1}{2}(1 + 1/\rho_0)}$ [12]. Then, the evolution of the fluid density and velocity until interaction occurs corresponds to two counterpropagating discontinuities with speeds $\pm v_0 = \pm \rho_0 u_0/(\rho_0 - 1)$ determined from jump conditions. At the time $t = t_1 = L/(2v_0)$ the two shocks overlap, giving the Riemann problem

$$\rho(x, t_1) = \rho_0, \quad u(x, t_1) = -\operatorname{sgn}(x)u_0,$$

with a step in u only. This can be solved exactly [12] to give two new VSWs propagating away from each other

$$\rho(x, t) = \begin{cases} \rho_0 & |x| > v_1(t - t_1) \\ \rho_m & |x| < v_1(t - t_1), \end{cases}$$
$$u(x, t) = \begin{cases} -u_0 \operatorname{sgn}(x) & |x| > v_1(t - t_1) \\ 0 & |x| < v_1(t - t_1), \end{cases}$$
$$\rho_m = \frac{1}{2}\left(\rho_0 - 1 + \sqrt{4\rho_0^3 + \rho_0^2 - 2\rho_0 + 1} \right),$$
$$v_1 = \frac{\rho_0 u_0}{\rho_m - \rho_0}.$$

Thus the collision of two classical VSWs results in two new counterpropagating VSWs with larger amplitude and different speed. The evolution of this collision process is shown in Fig. 30. Physically, this behavior can be understood as the collision of two counterpropagating volumes of gas, causing an increase in the gas density. Because gas continues to be fed into this region of higher density, two new shock fronts are created
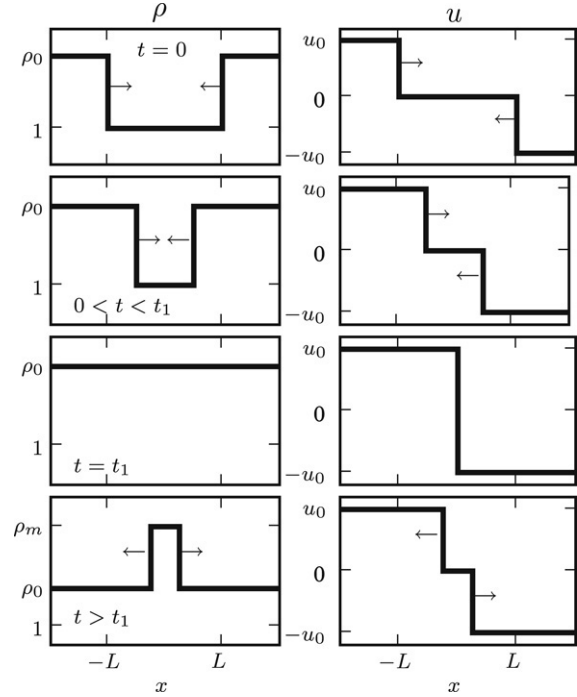
Fig. 30. Dissipative regularization of the Euler equations with a two shock collision. The overall behaviour of this collision process is qualitatively the same as what was found in the dispersive case for certain initial velocities, i.e. two shocks collide, interact and two new shocks with larger density amplitudes and altered speeds counterpropagate away from the collision region.

to carry the fluid away. In any physical system, the gas being fed into the region of higher density will eventually diminish in magnitude. So, this solution is physically valid as long as gas is continually fed into the region of higher density at near constant density and velocity. This qualitative behaviour is what was found for certain initial velocities ($-2\sqrt{\rho_0} + 2 < u_0 < 2\sqrt{\rho_0}$) in the dispersive case in Section 5.1.

Similar to the DSW case, interaction behaviour of VSWs depends on the choice of the initial velocity u_0. It is possible to generate, at each initial step, depending on the value of the initial velocity, (a) two rarefaction waves ($u_0 < -2\sqrt{\rho_0} + 2$), (b) one rarefaction and one shock ($-2\sqrt{\rho_0} + 2 < u_0 < (\rho_0 - 1)\sqrt{\frac{1}{2}(1 + \frac{1}{\rho_0})}$), or (c) two shock waves ($u_0 > (\rho_0 - 1)\sqrt{\frac{1}{2}(1 + \frac{1}{\rho_0})}$). The only difference from the canonical case is the possible interaction of a shock and rarefaction wave. One key difference between the classical and dispersive shock wave collision process is the generation of an interaction region that expands in time for the dispersive case (see Figs. 18 and 20). This is not possible in the classical case for any choice of initial velocity.

6.2. Merging

We now consider the dissipative regularization of the Euler Eqs. (44) with the initial data (37) and the pure shock conditions (see e.g. [12]),

$$u_1 = (\rho_1 - \rho_0)\frac{1}{\sqrt{2}}\left(\frac{1}{\rho_1} + \frac{1}{\rho_0} \right)^{\frac{1}{2}},$$
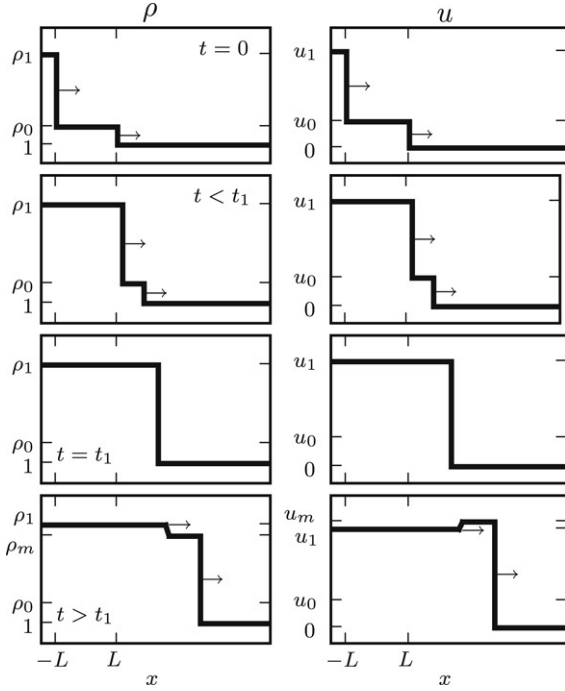
Fig. 31. The evolution of the density and velocity of a classical fluid with initial data (37). Two copropagating shocks are formed initially and eventually merge into a single shock with a rarefaction wave behind. Similar merging behavior (without the rarefaction wave) was also found when two DSWs interact.

$$u_0 = (\rho_0 - 1)\frac{1}{\sqrt{2}}\left(\frac{1}{\rho_0} + 1\right)^{\frac{1}{2}}.$$

Each of the two steps in the initial data can be solved individually for two VSWs. The shock speeds are determined from jump conditions, with the leftmost shock propagating with speed $v_- = (\rho_1 u_1 - \rho_0 u_0)/(\rho_1 - \rho_0)$, and the rightmost shock propagating with speed $v_+ = \rho_0 u_0/(\rho_0 - 1)$. Since $v_- > v_+$, the leftmost VSW eventually overtakes the rightmost VSW. At the instant when this occurs, $t_1 = 2L/(v_- - v_+)$ and $x_1 = L + v_+ t_1$, and we have a new Riemann problem to solve:

$$\rho(x, t_1) = \begin{cases} \rho_1 & x < x_1 \\ 1 & x > x_1, \end{cases} \quad u(x, t_1) = \begin{cases} u_1 & x < x_1 \\ 0 & x > x_1. \end{cases}$$

Solving this Riemann problem gives a small amplitude rarefaction wave connected via a constant region to a VSW propagating to the right [12]. The intermediate density ρ_m and velocity u_m are determined from the equations

$$u_1 + 2\left(\sqrt{\rho_1} - \sqrt{\rho_m}\right) = (\rho_m - 1)\frac{1}{\sqrt{2}}\left(\frac{1}{\rho_m} + 1\right)^{\frac{1}{2}},$$

$$u_m = u_1 + 2(\sqrt{\rho_1} - \sqrt{\rho_m}).$$

The classical merging of two VSWs is shown in Fig. 31. Except for the generation of a small amplitude rarefaction wave, this qualitative behaviour was also found in Section 5.2 for the case of two DSWs.

7. Conclusion

We examined the interaction of two dispersive shock waves by multiphase Whitham averaging and numerical simulation.

The agreement between asymptotic Whitham averaging theory (predicted 0-phase amplitudes and 0-phase/1-phase/2-phase boundaries) and full numerical simulation of the governing NLS equation is excellent.

The interaction process gives rise to a 2-phase interaction region. In the case of two counterpropagating DSWs that collide, this interaction region closes for a wide range of initial parameters. Two DSWs emerge from the interaction region and propagate away from each other with altered amplitudes and speeds. However, for large enough initial velocities, the 2-phase interaction region expands in time but is asymptotically ($t \to \infty$) degenerate. In the case of two copropagating DSWs analysed here, a single, *merged* DSW emerges from the interaction region. Apart from regions I and II, collisions with large initial velocity (see Fig. 5), we find that the long-time behaviour of dispersive shock wave interactions has many qualitative similarities to that of classical dissipative shock wave interactions.

References

[1] R.J. Taylor, D.R. Baker, H. Ikezi, Observation of collisionless electrostatic shocks, Phys. Rev. Lett. 24 (1970) 206–209.

[2] N.F. Smyth, P.E. Holloway, Hydraulic jump and undular bore formation on a shelf break, J. Phys. Oceanogr. 18 (7) (1988) 947–962.

[3] T.P. Simula, et al., Observations on sound propagation in rapidly rotating Bose-Eienstein condensates, Phys. Rev. Lett. 94 (2005) 080404.

[4] M.A. Hoefer, M.J. Ablowitz, I. Coddington, E.A. Cornell, P. Engels, V. Schweikhard, Dispersive and classical shock waves in Bose–Einstein condensates and gas dynamics, Phys. Rev. A (2006) 023623.

[5] W. Wan, S. Jia, J.W. Fleischer, Dispersive superfluid-like shock waves in nonlinear optics, Nat. Phys. 3 (2007) 46–51.

[6] A.V. Gurevich, L.P. Pitaevskii, Nonstationary structure of a collisionless shock wave, Sov. Phys. JETP 38 (2) (1974) 291–297.

[7] A.V. Gurevich, A.L. Krylov, Dissipationless shock waves in media with positive dispersion, Sov. Phys. JETP 65 (5) (1987) 944–953.

[8] A.M. Kamchatnov, Nonlinear Periodic Waves and Their Modulations: An Introductory Course, World Scientific, River Edge, NJ, 2000.

[9] G.A. El, Resolution of a shock in hyperbolic systems modified by weak dispersion, Chaos 15 (2005) 037103.

[10] R. Courant, K.O. Friedrichs, Supersonic Flow and Shock Waves, Springer-Verlag, 1948.

[11] P.D. Lax, Hyperbolic Systems of Conservation Laws and the Mathematical Theory of Shock Waves, SIAM, 1973.

[12] R.J. LeVeque, Finite Volume Methods for Hyperbolic Problems, Cambridge University Press, 2002.

[13] G.B. Whitham, Non-linear dispersive waves, Proc. Roy. Soc. Ser. A 283 (1965) 238–261.

[14] M.J. Ablowitz, D.J. Benney, The evolution of multi-phase modes for nonlinear dispersive waves, Stud. Appl. Math. 49 (1970) 225–238.

[15] H. Flaschka, M.G. Forest, D.W. McLaughlin, Multiphase averaging and the inverse spectral solution of the Korteweg-de Vries equation, Comm. Pure Appl. Math. 33 (1980) 739–784.

[16] M.G. Forest, J. Lee, Geometry and modulation theory for the periodic nonlinear Schrödinger equation, in: C. Dafermos, et al. (Eds.), Oscillation Theory, Computation, and Methods of Compensated Compactness, vol. 2, Springer, 1986, pp. 35–69.

[17] Y. Kodama, The Whitham equations for optical communications: Mathematical theory of NRZ, SIAM J. Appl. Math. 59 (6) (1999) 2162–2192.

[18] G. Biondini, Y. Kodama, On the Whitham equations for the defocusing nonlinear Schrödinger equation with step initial data, J. Nonlinear Sci. 16 (2006) 435–481.

[19] G.A. El, V.V. Geogjaev, A.V. Gurevich, A.L. Krylov, Decay of an initial discontinuity in the defocusing NLS hydrodynamics, Physica D 87 (1995) 186.

[20] V. Perez-Garcia, H. Michinel, H. Herrero, Bose–Einstein solitons in highly asymmetric traps, Phys. Rev. Lett. 57 (1998) 3837.

[21] R.W. Boyd, Nonlinear Optics, Academic Press, San Diego, CA, 2003.

[22] S. Jin, C.D. Levermore, D.W. McLaughlin, The behavior of solutions of the NLS equation in the semiclassical limit, in: N.M. Ercolani, et al. (Eds.), Singular Limits of Dispersive Waves, vol. 320, Plenum Press, 1994, pp. 235–255.

[23] M.V. Pavlov, Nonlinear Schrödinger equation and the Bogolyubov–Whitham method of averaging, Teor. Mat. Fiz. 71 (3) (1987) 351–356.

[24] E.D. Belokolos, A.I. Bobenko, V.Z. Enolski, A.R. Its, V.B. Matveev, Algebro-geometric Approach to Nonlinear Integrable Equations, Springer, New York, 1994.

[25] Y.C. Ma, M.J. Ablowitz, The periodic cubic Schrödinger equation, Stud. Appl. Math. 65 (1981) 113–158.

[26] P.F. Byrd, M.D. Friedman, Handbook of Elliptic Integrals for Engineers and Physicists, Springer-Verlag, 1954.

[27] J. Frauendiener, C. Klein, Hyperelliptic theta functions and spectral methods, J. Comp. Appl. Math. 167 (2004) 193.

[28] L.N. Trefethen, Spectral Methods in Matlab, SIAM, 2000.

[29] SciPy, software for mathematics, science, and engineering. www.scipy.org.

[30] J.A.C. Weideman, B.M. Herbst, Split-step methods for the solution of the nonlinear Schrödinger equation, SIAM J. Numer. Anal. 23 (1986) 485–507.

[31] M.J. Ablowitz, H. Cornille, On solutions of the Korteweg-de Vries equation, Phys. Lett. 72A (1979) 277–280.

[32] P.M. Santini, M.J. Ablowitz, A.S. Fokas, The direct linearization of a class of nonlinear evolution equations, J. Math. Phys. 25 (1984) 2614–2619.

[33] T. Grava, F.-R. Tian, The generation, propagation, and extinction of multiphases in the KdV zero-dispersion limit, Comm. Pure Appl. Math. 55 (12) (2002) 1569–1639.

[34] J. Kevorkian, Partial Differential Equations, Analytical Solution Techniques, second ed., Springer, New York, NY, 2000.